Chemical Engineering Journal 436 (2022) 135201

Contents lists available at ScienceDirect

Chemical Engineering Journal

journal homepage: www.elsevier.com/locate/cej

# Deciphering the simultaneous removal of carbamazepine and metronidazole by monolithic $Co_2AlO_4@Al_2O_3$ activated peroxymonosulfate

Min-Ping Zhu [a,b], Jia-Cheng E. Yang [a,*], Darren Delai Sun [c], Baoling Yuan [d], Ming-Lai Fu [a,d,*]

[a] Key Laboratory of Urban Pollutant Conversion, Institute of Urban Environment (IUE), Chinese Academy of Sciences (CAS), No. 1799, Jimei Avenue, Xiamen 361021, PR China
[b] University of Chinese Academy of Sciences (UCAS), No. 19(A), Yuquan Road, Shijingshan District, Beijing 100049, PR China
[c] School of Civil and Environmental Engineering, Nanyang Technological University, 639798, Singapore
[d] Xiamen Key Laboratory of Municipal and Industrial Solid Waste Utilization and Pollution Control, College of Civil Engineering, Huaqiao University, Xiamen 361020, PR China

ARTICLE INFO

*Keywords:*
Carbamazepine
Metronidazole
$Co_2AlO_4$
Emerging contaminants
Wastewater decontamination/detoxification

ABSTRACT

Reported here is a pioneering work on the co-removal of carbamazepine (CBZ) and metronidazole (MNZ) by $Co_2AlO_4@Al_2O_3$ millispheres activated peroxymonosulfate (PMS). Compared with the single removal, the reduced ratios for the removal kinetics of MNZ (72.16%) are two times higher than that of CBZ (35.41%) within initial pH 3 – 9. This is essentially due to the higher oxidation affinity of $SO_4^{\bullet-}$ and $^1O_2$ toward CBZ than MNZ. $Cl^-$ facilitated the degradation of CBZ but inhibited the degradation of MNZ, probably ascribed to the formation of HOCl and $Cl_2^{\bullet-}$. $HCO_3^-$ and $PO_4^{3-}$ significantly inhibited the removal of CBZ and MNZ by scavenging $SO_4^{\bullet-}$ and/or passivating the active sites of $Co_2AlO_4@Al_2O_3$. The degradation of CBZ is mainly due to the electron abstraction and oxygen addition, while the primary oxidation processes of MNZ include the denitration, ring opening and/or N-C cleavage. Because of the competition of CBZ against $SO_4^{\bullet-}$, the simultaneous removal process remarkably changed the main products of MNZ compared with the single removal process. The simultaneous removal of CBZ and MNZ increased the total bioaccumulation potential and mutagenicity risk of degradation products but helped to reduce their total developmental toxicity. The products formed in the co-removal process showed higher total acute toxicity to *Daphnia magna* than those of the single process, while for the total acute toxicity to *Oral rat*, the results are reversed. This work will spark more interest of simultaneously removing multiple emerging pollutants with monolithic catalysts-oriented oxidation processes.

## 1. Introduction

The ubiquity of pharmaceuticals (a group of emerging contaminants) in the ground waters, surface waters and/or wastewater effluents constitutes a serious threat to the access to drinking water and the security of ecosystem [1,2]. With the ever-increasing interest in developing diverse techniques/methods to remove pharmaceuticals [3–5] and the mounting evidence of various pharmaceuticals concurrently present in the wastewater effluents [3,6], the focus of removing pharmaceuticals has gradually shifted from the individual removal to the simultaneous elimination [7,8]. Although the second-order reaction rate constants of pharmaceuticals with reactive radicals (like $SO_4^{\bullet-}$, $^{\bullet}OH$ and $Cl^{\bullet}$) had been well documented [9,10], the prediction on the simultaneous removal of multiple pharmaceuticals by advanced oxidation process (AOP) cannot be achieved and is still up in the air. This is due to the complexity of drug-drug interactions (competing for various reactive radicals) and the variability of degradation pathways [8,11]. Besides the diversity of reactive oxygen species (ROS) and the structure variability of pollutants, complex water matrix conditions are another factor which can affect the simultaneous removal of multiple pharmaceuticals. For example, the secondary reactive species (like $Cl^{\bullet}/Cl_2^{\bullet}$ and $CO_3^{\bullet-}$, resulted from the reactions of $SO_4^{\bullet-}/^{\bullet}OH$ with $Cl^-$ and $HCO_3^-$ in the wastewaters) may also participate in the degradation of pharmaceuticals [10,12], which would complicate the simultaneous removal and even result in toxic byproducts. In this context, developing a cost-effective method to simultaneously eliminate multiple pharmaceuticals is challenging but of great importance to practical water purification.

The radicals-centered chemical oxidation has been considered a

* Corresponding Authors.
*E-mail addresses:* jcyang@iue.ac.cn (J.-C.E. Yang), mlfu@iue.ac.cn, mlfu@hqu.edu.cn (M.-L. Fu).

https://doi.org/10.1016/j.cej.2022.135201
Received 12 November 2021; Received in revised form 15 January 2022; Accepted 8 February 2022
Available online 12 February 2022

promising technique to completely degrade the pharmaceuticals, especially in comparison to either physicochemical adsorption and biodegradation processes [13,14]. The latest popularity of persulfates (PS)-based AOP in degrading/removing pharmaceuticals lies in the formation of highly reactive $SO_4^{\bullet-}$ (2.5 – 3.1 $V_{NHE}$) and $^{\bullet}OH$ (1.7 – 2.8 $V_{NHE}$) for water detoxification [15]. Among all the metal-based catalysts for persulfate activation, metal organic frameworks (MOFs) and their derivatives have become the stars of activating peroxymonosulfate (PMS, $HSO_5^-$) or peroxydisulfate (PDS, $S_2O_8^{2-}$) to generate highly reactive oxidants [16–22]. The well-designed ZIF-67 and ZIF-67 derived $Co_3O_4$ composites were shown to decompose PMS and PDS into highly reactive radicals for eliminating various pharmaceuticals [16,20]. Meanwhile, to overcome the bottleneck of using micro/nano-sized MOFs-based composites for catalytically removing pharmaceuticals, recent attention has been directed in constructing the monolithic MOFs-oriented macro-catalysts for persulfate activation [23–27]. However, our understanding of the catalytical elimination of pharmaceuticals by MOFs-based catalysts is still based on the individual removal of pollutants [16,20,23,28]. There exists a paucity of knowledge regarding simultaneous removal of multiple pharmaceuticals by the activated persulfates with MOFs-based catalysts. Undoubtedly, this lack of knowledge will either overrate or underestimate the practical performance of MOFs-oriented PS-AOPs for eliminating multiple pharmaceuticals.

Bearing these issues in mind, we unprecedentedly reported the simultaneous removal of carbamazepine (CBZ) and metronidazole (MNZ) using monolithic $Co_2AlO_4$@$Al_2O_3$ (MCA) pellets as the activators of PMS. The removal of CBZ and MNZ from the single and binary solutions by MCA/PMS were comparably studied to better understand their competitive degradation with respect to the oxidation kinetics, reaction mechanisms and product toxicity. The simultaneous removal profiles of CBZ and MNZ under different initial solution pH and coexisting inorganic anions were systematically examined. CBZ and MNZ were selected as the model pharmaceuticals with the following reasons [1]: I) CBZ and MNZ are two N-containing pharmaceuticals widely coexisted in the river, wastewater treatment plant and hospital effluents. II) CBZ is an antipsychotic medication with an electron-donating group of $–NH_2$, while MNZ is an antibiotic/antiprotozoal with an electron-withdrawing group of $–NO_2$. We hypothesize that the structure diversity of CBZ and MNZ would result in the diverse competing abilities for ROS over their simultaneous removal process. To our best of knowledge, reported here is the first example of using monolithic MOFs-oriented catalysts for catalytically eliminating two classes of pharmaceuticals simultaneously. We believe that results from this work will spark more interests of developing multifunctional MOFs-oriented macro-catalysts for the purpose of simultaneously removing multiple pharmaceuticals.

## 2. Materials and methods

### 2.1. Materials

Monolithic $Co_2AlO_4$@$Al_2O_3$ (MCA) pellets used in this work can be synthesized via our previous methods [29] and the details can be found in Text S1. The starting materials, γ-$Al_2O_3$ (3 – 5 mm in diameter, CAS No. 1344–28-1) and cobalt nitrate hexahydrate ($Co(NO_3)_2{\cdot}6H_2O$) were provided by Sinopharm, whereas 2-methylimidazole (2-MIM) were obtained from Aladdin. The target pollutants, metronidazole (MNZ, CAS No. 443–48-1) and carbamazepine (CBZ, CAS No. 298–46-4) were also purchased from Aladdin. Unless otherwise noted, all the chemicals were used without any purification.

### 2.2. Degradation experiments

Individual removal and co-removal profiles of CBZ (10 mg/L) and MNZ (10 mg/L) by MCA/PMS were investigated under different initial pH values (3, 5, 7 and 9), anions ($Cl^-$, $NO_3^-$, $HCO_3^-$, $SO_4^{2-}$ and $PO_4^{3-}$) and quenchers (ethanol (EtOH), *tert* butyl alcohol (TBA), p-benzoquinone (BQ) and L-histidine (HD). The initial pH of single CBZ solution (SCS), single MNZ solution (SMS) and binary CBZ-MNZ solution (BZS) were adjusted using a dilute $H_2SO_4$ or NaOH solution. To avoid the interference against PMS activation, we failed to use the buffering substances like to maintain solution pH [30]. All the degradation experiments were conducted in 100-mL conical flasks with glass stoppers. Firstly, 80 mL of target solutions and 1.6 g of MCA (20 g/L) were introduced into the flaks. Then, PMS stock solution was introduced into the flacks to trigger the reaction in an orbital shaker (300 rpm, 25 ± 1 °C). At the specific time intervals, 1 mL of the samples were withdrawn and promptly quenched by 0.25 mL of EtOH. Prior to analysis, the samples were filtered through a 0.22 μm membrane filter and stored in the 4 °C-refrigerator. The used MCA samples were separated without any post-treatment, and directly used in the next run to evaluate their reusability. The concentrations of Co ions released from MCA and the solution pH values after reaction were measured. For comparison, the individual removal and co-removal of CBZ and MNZ by sole PMS under different initial pH values and anions were also studied. Each experiment has two duplicates. The average value with deviation was presented.

### 2.3. Analytical methods

The residual concentrations of CBZ and MNZ were determined by a high-performance liquid chromatography system (HPLC, Agilent 1260, USA), equipped with a diode array detector and an Agilent Poreshell 120 EC-C18 column (4.6 × 250 mm, 4 μm). The mobile phase consisting of acetonitrile (A) and ultrapure water (B) was employed to analyze CBZ (50:50, v:v) of A and B) and MNZ (20:80, v:v) of A and B). The detection wavelengths for CBZ and MNZ are 286 nm and 318 nm, respectively. After 60 min reaction, the degradation products of CBZ and MNZ in the single or binary solution were determined using a HPLC-MS/MS system (Q-Exactive Ultimate 3000 UPLC, Thermo Scientific, USA). The transformation product of CBZ with a molecular weight of *W* ($m/z + 1$ or $– 1$ based on the detection MS model) and a retention time of *t* (min) was denoted as C*W-t*. Analogously, M*W-t* stands for a transformation product of MNZ in the single or binary solution. The proportion of C*W-t* (or M*W-t*) in the single or binary solution was calculated based on the peak area of each product. The concentrations of Co ions released from MCA were detected by an inductively coupled plasma optical emission spectrometry (ICP-OES, Optima 7000DV, PerkinElmer, USA). The Toxicity Estimation Software Tool (T.E.S.T) was used to calculate the toxicity of C*W-t*, M*W-t*, CBZ and MNZ. The specific toxicity index, including bioaccumulation factor, development toxicity, mutagenicity, *Daphnia magna* LC50 (LC50) and *Oral rat* LD50 (LD50), was obtained based on the quantitative structure–activity relationship (QSAR) method. With respect to a specific toxicity index, the normalized total toxicity of all products ($T_{st,NT}$) in the single or binary solution was introduced as follows [31]:

$$T_{st,\ NT} = \Sigma_1^{\text{All products}} (T_{st,P}{}^{*} f_P) \quad \text{(a)}$$

where $f_P$ is the relative ratio of one product in the single or binary solution (e.g., 71.51% for *C252-10.3* in the single CBZ solution), $T_{st,P}$ is a special toxicity value of one product (e.g., the LC50 value of *C252-10.3* to *Daphnia magna* is 2.82 mg/L).

## 3. Results and discussion

### 3.1. Competitive degradation of CBZ and MNZ by MCA/PMS

Fig. 1 shows the individual and simultaneous removal of CBZ and MNZ by MCA activated PMS. Control experiments show that, whether in the single or binary system, sole PMS can hardly remove CBZ and MNZ. Moreover, MCA also showed limited adsorption toward the individual and simultaneous removal of CBZ and MNZ (Fig. 1). Evidently, the combination of PMS and MCA remarkably enhanced the removal of CBZ

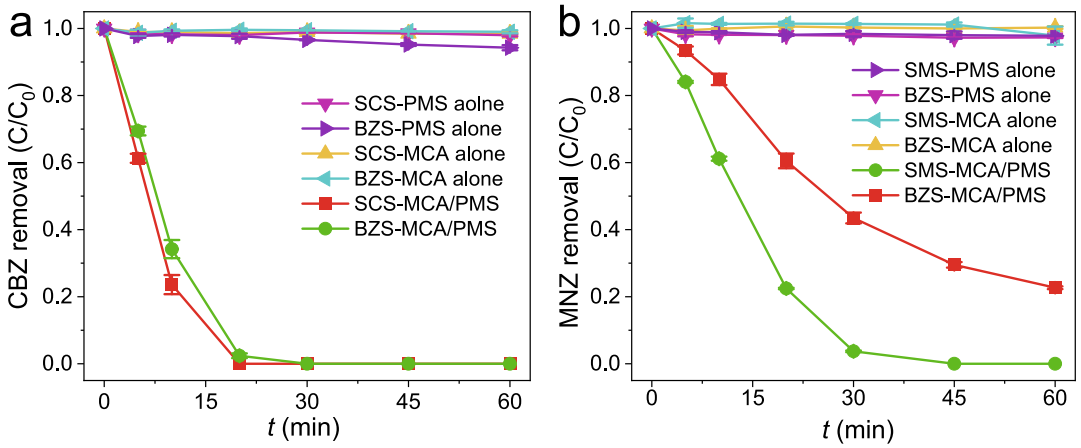


**Fig. 1.** The removal of CBZ (a) and MNZ (b) by monolithic $Co_2AlO_4$@$Al_2O_3$ (MCA)/PMS from the single CBZ solution (SCS), single MNZ solution (SMS) and binary CBZ-MNZ solution (BZS) ([MCA] = 20 g/L, [CBZ] = [MNZ] = 10 mg/L, [PMS] = 1.0 mM, initial pH = 7.0, T = 25 ± 1 °C).

and MNZ. For instance, complete removal of CBZ from the SCS was achieved within 20 min, and the corresponding pseudo-first-order kinetic constant ($k_{obs}$) reached 1.35 × $10^{-1}$ $min^{-1}$ (Table S1). MNZ in the SMS was completely removed at 45 min, and the corresponding $k_{obs}$ value was 9.44 × $10^{-2}$ $min^{-1}$ (Table S1). Interestingly, for the co-removal of CBZ and MNZ, the existence of MNZ slightly decreased the removal of CBZ (Fig. 1a), whereas the presence of CBZ caused a significant inhibition to the removal of MNZ (Fig. 1b). The $k_{obs}$ value for the removal of MNZ from BZS was decreased by 72.14% (from 9.44 × $10^{-2}$ to 2.63 × $10^{-2}$ $min^{-1}$) (Table S1). The findings suggest that CBZ is more likely to be degraded than MNZ by the MCA/PMS system, and that the degradation of CBZ in the binary solution seems to be a priority. We considered that there exist two reasons: (1) the different groups of CBZ and MNZ molecules, (2) the selective attack of ROS toward CBZ and MNZ molecules (as shown in Section 3.5).

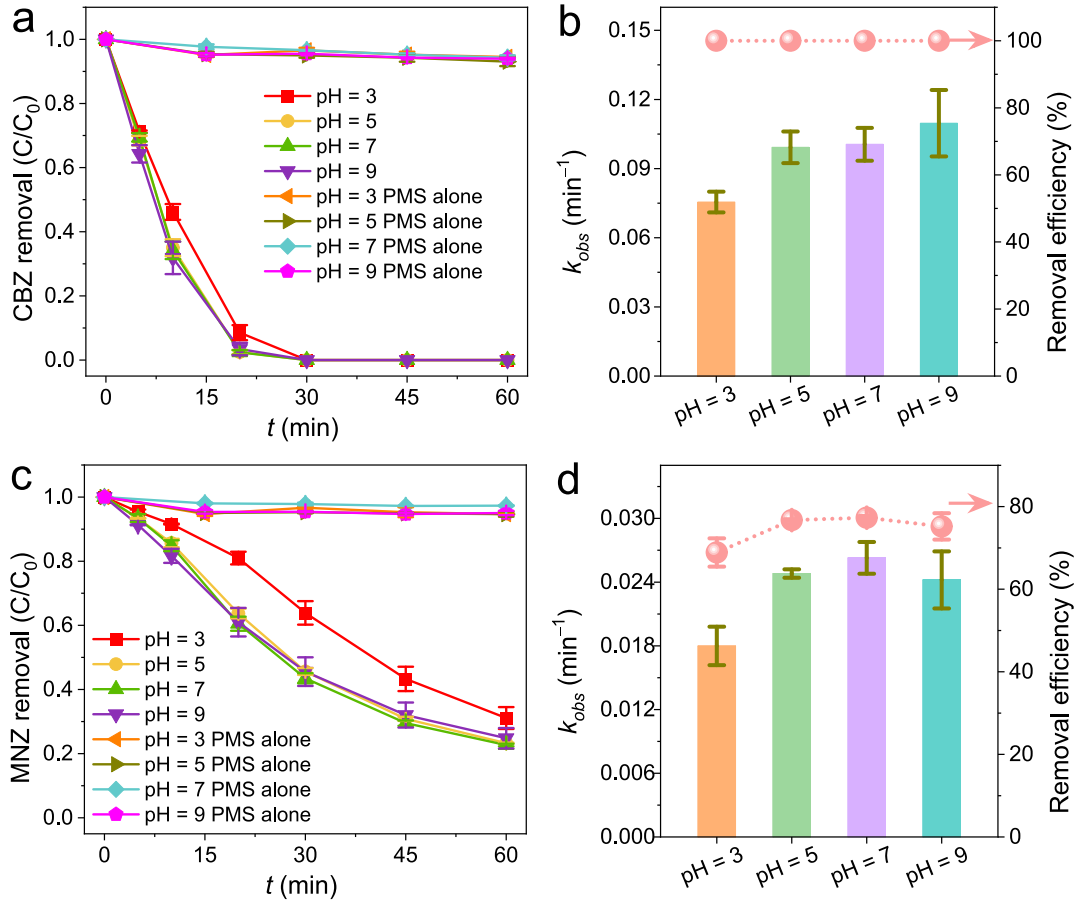


**Fig. 2.** Effect of initial pH on the simultaneous removal of CBZ (a, b) and MNZ (c, d) from the binary CBZ-MNZ solution ([MCA] = 20 g/L, [CBZ] = [MNZ] = 10 mg/L, [PMS] = 1.0 mM, T = 25 ± 1 °C).

### 3.2. Effect of initial pH

As depicted in Fig. 2 and Fig. S1, the simultaneous and individual removal of CBZ and MNZ by the sole oxidation of PMS can be neglected in the pH range of 3.00 – 9.00. With the initial solution pH increased, the removal efficiencies of CBZ in the binary solutions were barely affected with the corresponding $k_{obs}$ values being slightly increased (Fig. 2a, b). This is similar to the trends for the removal of CBZ from the SCS with the same pH range (Fig. S1a, b). Compared with the single solution, the $k_{obs}$ values for the removal of CBZ from the binary solution were decreased by 22.94% – 35.47% (cf. Table S1). Generally, the $k_{obs}$ values for the removal of MNZ from SMS and BZS were firstly increased and then decreased with the solution pH increased (Fig. 2c, d and Fig. S1c, d). The presence of CBZ in BZS significantly reduced the $k_{obs}$ values of MNZ (by 59.18% – 72.16%) (cf. Table S1). This is probably due to the competition effects of CBZ and MNZ with ROS and the selectivity of ROS toward them. In general, the co-removal of CBZ and MNZ by MCA/PMS was slightly influenced by the initial solution pH itself, except for the pH 3.00, which was also observed for the removal of CBZ and MNZ in their single solutions (Fig. 2, Fig. S1). We think that the less $Co(OH)^+$ species (caused by the lower pH 3.00), retarded the formation of reactive radicals over PMS activation by MCA [32], thus reducing the oxidation kinetics of CBZ and MNZ (cf. Fig. 2). Our primary experiments indicate that after adding PMS, the pH values of single or binary solutions will experience a significant decrease and then reach a plateau within 15 min. It is clear that, after adding PMS and MCA, the solution pH fell into the range of 3.68 – 4.28 for the single or binary system in the absence of inorganic ions (Table S1). Under this case, MCA was positively charged according to the surface charge of MCA as a function of pH (Fig. S2), which helped to activate/decompose the negative PMS ($HSO_5^-$) for producing ROS. From the view of electrostatic interaction, $SO_4^{\bullet-}$ is theoretically prone to attack the positive CBZ ($pK_a$ = 13.94) compared with the negative MNZ ($pK_{a1}$ = 2.40) [33,34]. Therefore, we consider that the difference in the $pK_a$ of CBZ and MNZ is also an importance factor affecting their simultaneous removal.

### 3.3. Effect of inorganic anions

The individual and simultaneous removal behaviors of CBZ and MNZ by the MCA/PMS system were further investigated under different common inorganic anions, i.e., $Cl^-$, $SO_4^{2-}$, $PO_4^{3-}$, $HCO_3^-$, and $NO_3^-$ (Fig. 3, Table S1). Interestingly, $Cl^-$ exhibited dual effects on the co-removal of CBZ and MNZ. Specially, the presence of $Cl^-$ (10 mM) dramatically facilitated the oxidation of CBZ, but on the other side, almost completely inhibited the degradation of MNZ (Fig. 3). The corresponding $k_{obs}$ value for the degradation of CBZ ($6.62 \times 10^{-1}$ $min^{-1}$) was about 6.55 times higher than that without $Cl^-$ ($1.01 \times 10^{-1}$ $min^{-1}$). For the degradation of MNZ, the addition of 10 mM $Cl^-$ in the binary solution significantly decreased its $k_{obs}$ value from $2.63 \times 10^{-2}$ $min^{-1}$ to $1.30 \times 10^{-3}$ $min^{-1}$ (more than 20 times). We think that the peculiar influences of $Cl^-$ on the co-removal of CBZ and MNZ could be due to the possible reasons: i) the formation of secondary radicals (i.e., $Cl^{\bullet}$, $Cl_2^{\bullet-}$, and $HOCl^{\bullet-}$) from the reactions between $Cl^-$ and $SO_4^{\bullet-}$ in the MCA/PMS system [35] (cf. Reaction 1 – 4), ii) the formation of HOCl from the direct reaction of $Cl^-$ with PMS [36] (Reaction 5), and iii) the different oxidation potential of chloride-based active species toward CBZ and MNZ [9,37]. With respect to the removal of CBZ and MNZ, the role of $Cl^{\bullet}$ formed in the $Cl^-$-containing MCA/PMS system can be excluded. In

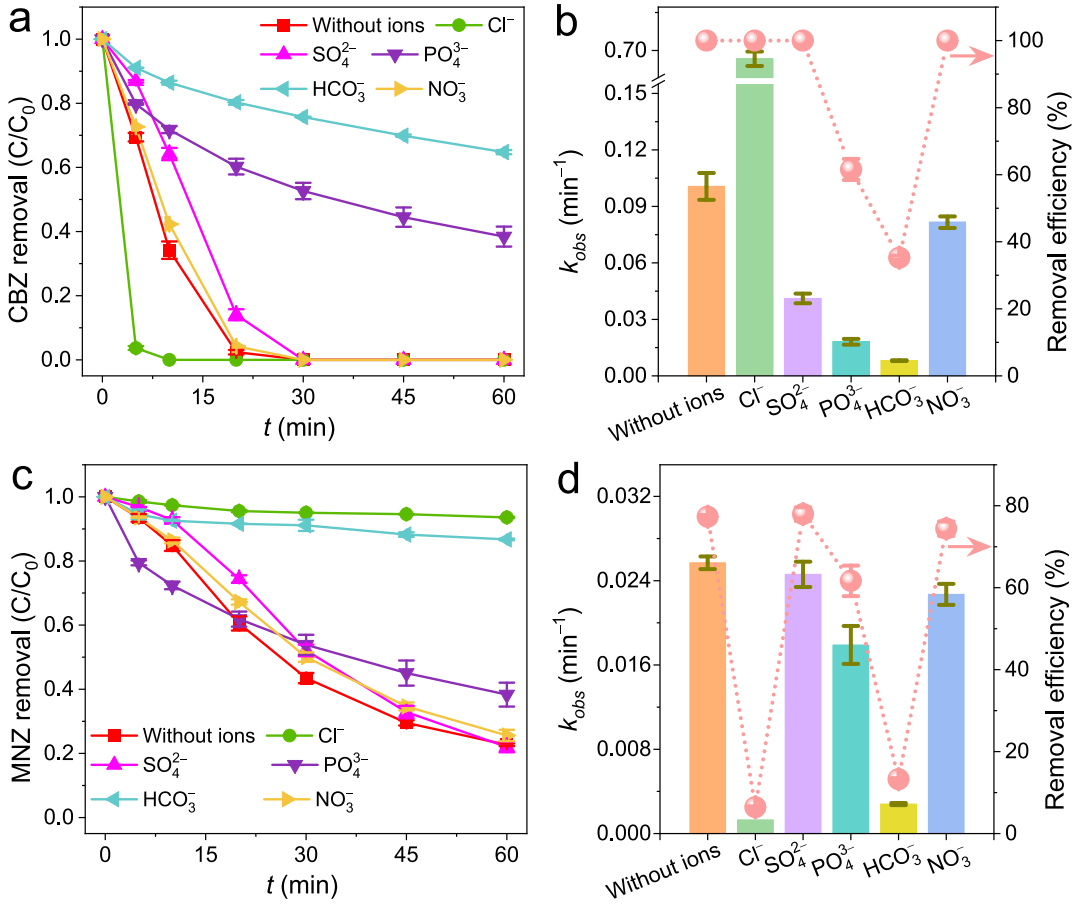


**Fig. 3.** Effect of co-existing inorganic ions on the simultaneous removal of CBZ (a, b) and MNZ (c, d) in the binary CBZ-MNZ solution ([MCA] = 20 g/L, [CBZ] = [MNZ] = 10 mg/L, [PMS] = 1.0 mM, initial pH = 7.0, T = 25 ± 1 °C).

theory, the formation of $Cl^{\bullet}$ would increase the oxidation kinetics of both CBZ and MNZ because the second-order reaction rate constants of $Cl^{\bullet}$ with CBZ ($3.30 \times 10^{10}$ $M^{-1}\bullet s^{-1}$) and MNZ ($3.10 \times 10^{9}$ $M^{-1}\bullet s^{-1}$) are higher than those of $SO_4^{\bullet-}$ with CBZ ($1.92 \times 10^{9}$ $M^{-1}\bullet s^{-1}$) and MNZ ($2.74 \times 10^{9}$ $M^{-1}\bullet s^{-1}$) [9,37]. However, the removal of MNZ from the binary or single solution suffered from a distinctive decrease (Fig. 3c, d and Fig. S3c, d). The insignificant role of $Cl^{\bullet}$ was probably due to its low steady-state concentration in the $Cl^-$/MCA/PMS system, resulted from the fast reaction of $Cl^{\bullet}$ with $Cl^-$ (to form $Cl_2^{\bullet-}$) or the subsequent self-quenching of $Cl_2^{\bullet-}$ (to form HOCl under the condition of excessive $Cl^-$) (cf. Reaction 3 – 4). The second-order reaction rate constant of $Cl_2^{\bullet-}$ with MNZ ($1.24 \times 10^{8}$ $M^{-1}\bullet s^{-1}$) was found to be one order magnitude lower than those of $SO_4^{\bullet-}$/$Cl^{\bullet}$ with MNZ [9]. Therefore, the formation of $Cl_2^{\bullet-}$ might cause the lower removal kinetics of MNZ in the single or binary solution. Note that without MCA, CBZ in the binary solution can also be degraded by the sole PMS with the presence of 10 mM $Cl^-$, and more than 81.00% of CBZ was removed within 15 min (Fig. S4a). This phenomenon is likely attributed to the generation of HOCl ($E^0 = 1.48$ $V_{NHE}$) from the direct reaction of $Cl^-$ with PMS (refer to Reaction 5) [36], which can effectively degrade CBZ [38]. On the contrary, the reaction of $Cl^-$ with PMS to form HOCl cannot degrade MNZ (Fig. S4b). This is probably due to the presence of $–NO_2$ group within MNZ, which is less vulnerable to the attack of HOCl than the $–NH_2$ group within CBZ [39–41]. Compare with $Cl_2^{\bullet-}$ relying on the formation of primary $SO_4^{\bullet-}$, the formation of HOCl in the $Cl^-$/MCA/PMS system should be faster due to the nature of homogenous reaction of $Cl^-$ with PMS. In all, the co-removal of CBZ and MNZ by the $Cl^-$/MCA/PMS system much depends on both the primary radical/chloride species and the intrinsic molecular structures/properties of target pollutants.

Although $HCO_4^-$ ($E^0 = 1.8$ $V_{NHE}$) can be produced from the reaction of $HCO_3^-$ and PMS (refer to Reaction 6) [36], the presence of 10 mM $HCO_3^-$ in the binary solution exhibited distinct inhibitory impacts on the co-removal of CBZ and MNZ (Fig. 3). Compared with the binary solution without $HCO_3^-$, the addition of $HCO_3^-$ resulted in the $k_{obs}$ values of CBZ and MNZ being decreased by 91.98% and 89.07%, respectively. Analogously, the presence of $HCO_3^-$ in the single solution of CBZ and MNZ caused the corresponding $k_{obs}$ values being reduced by 93.39% and 92.24%, respectively (Fig. S3, Table S1). These phenomena could be explained by the scavenger reactions of $HCO_3^-$ with $SO_4^{\bullet-}$ (Reaction 7), which can result in the formation of $CO_3^{\bullet-}$. The resultant $CO_3^{\bullet-}$ is a highly selective oxidant preferring to attack the electron-rich aromatic pollutants [12]. Therefore, the transformation of $SO_4^{\bullet-}$ into $CO_3^{\bullet-}$ is considered as the probable reason for the decreased removal of CBZ and MNZ by the $HCO_3^-$/MCA/PMS system. Compared with $HCO_3^-$, the presence of $PO_4^{3-}$ induced less inhibition toward the removal of CBZ and MNZ (Fig. 3). For the $PO_4^{3-}$/MCA/PMS system, the $k_{obs}$ values for the co-removal of CBZ and MNZ were decreased by 81.97% and 30.26%, respectively, compared with the $PO_4^{3-}$-free MCA/PMS system. For the single solution of CBZ and MNZ, the presence of $PO_4^{3-}$ also resulted in the $k_{obs}$ values of CBZ and MNZ being decreased by 79.39% and 47.93%, respectively (Fig. S3, Table S1). Previous study revealed that PMS tends to be pre-activated by $PO_4^{3-}$ [42], which can be also verified by the elimination of 13.63% CBZ and 10.94% MNZ in the $PO_4^{3-}$/PMS system (Fig. S4a, b). Nevertheless, $PO_4^{3-}$ could also work as a scavenger for $SO_4^{\bullet-}$ (Reaction 8 – 10), thus leading to decreased oxidation potential toward CBZ and MNZ. It is clear that, the inhibition effects of $NO_3^-$ and $SO_4^{2-}$ on the co-removal of CBZ and MNZ were much weaker than those of $HCO_3^-$ and $PO_4^{3-}$ (Fig. 3). Besides their scavenging effect, the complexation of $HCO_3^-$ and $PO_4^{3-}$ with the Co species would also deteriorate the catalytic activity of MCA in PMS activation and thus the removal of CBZ and MNZ [35,43].

$Cl^- + SO_4^{\bullet-} \rightarrow Cl^{\bullet} + SO_4^{2-}$ (1)

$Cl^- + Cl^{\bullet} \leftrightarrow Cl_2^{\bullet-}$ (2)

$2Cl_2^{\bullet-} \rightarrow Cl_2 + 2Cl^-$ (3)

$Cl_2^{\bullet-} + H_2O \rightarrow HOCl^{\bullet-} + Cl^- + H^+$ (4)

$Cl^- + HSO_5^- \rightarrow HOCl + SO_4^{2-}$ (5)

$HCO_3^- + HSO_5^- \rightarrow HCO_4^- + HSO_4^-$ (6)

$HCO_3^- + SO_4^{\bullet-} \rightarrow SO_4^{2-} + CO_3^{\bullet-} + H^+$ (7)

$PO_4^{3-} + H_2O \rightarrow HPO_4^{2-} + OH^-$ (8)

$HPO_4^{2-} + H_2O \rightarrow H_2PO_4^- + OH^-$ (9)

$HPO_4^{2-} + SO_4^{\bullet-} \rightarrow SO_4^{2-} + HPO_4^{\bullet-}$ (10)

### 3.4. Effect of MCA reusability

The effect of MCA reusability on the removal of CBZ and MNZ is shown in Fig. S5. Whether in the single or binary solution, the removal kinetics of CBZ and MNZ was gradually decreased with the increase of reuse times. The $k_{obs}$ values for the removal of MNZ from the binary solution in the first, second, third and fourth recycle of MCA are $2.43 \times 10^{-2}$ $min^{-1}$, $8.55 \times 10^{-3}$ $min^{-1}$, $5.95 \times 10^{-3}$ $min^{-1}$ and $3.20 \times 10^{-3}$ $min^{-1}$, respectively, and those for the case of single MNZ solution are $7.46 \times 10^{-2}$ $min^{-1}$, $2.98 \times 10^{-2}$ $min^{-1}$, $2.18 \times 10^{-2}$ $min^{-1}$ and $1.11 \times 10^{-2}$ $min^{-1}$, respectively. By contrast, the decrease in the removal of CBZ is much weaker than that of MNZ. For example, the removal efficiencies of CBZ from the binary or single solutions in the first three recycle can reach 97.24% and 100.00% respectively, while those of MNZ are 33.84% and 76.92%, respectively. We think that the higher removal kinetics and efficiency of CBZ than MNZ in the recycling experiments mainly lies in the preferential oxidation of ROS toward CBZ due to its electron-donating group and positive charge [44]. In general, the decreased ratio of $Co^{3+}/Co^{2+}$ species within MCA and the coverage of oxidation products on the active sites of MCA are probably the main reasons affecting the activity of the used MCA in PMS activation (cf. Table 1).

### 3.5. ROS-regulated degradation mechanism

Types of ROS and their contribution

The single and simultaneous removal behaviors of CBZ and MNZ by the MCA/PMS system with various scavengers were systematically studied to examine the types of ROS and understand the co-removal/co-degradation mechanisms of CBZ and MNZ. The commonly used quenchers, such as *tert*-butanol (TBA), ethanol (EtOH), *L*-histidine (HD) and *p*-benzoquinone (BQ) were employed to distinguish $SO_4^{\bullet-}$, $^{\bullet}OH$, $O_2^{\bullet-}$ and $^1O_2$ in this work [45]. Although HD and BQ have the ability to decompose PMS under the buffering condition (maintaining solution pH above 7) [46,47], our previous work indicates that, without buffering, the reaction of HD and BQ with PMS cannot be considered as the main reason for the PMS decomposition [31]. Considering the high reaction rate of BQ and HD with $SO_4^{\bullet-}$ and $^{\bullet}OH$ ($10^8 – 5 \times 10^9$ $M^{-1}\bullet s^{-1}$) [31], we qualified the relative contribution of $O_2^{\bullet-}$ and $^1O_2$ by comprehensively analyzing the effects of EtOH, TBA, HD and/or BQ (rather than the sole effect of BQ or HD). As shown in Fig. 4a, b, the removal efficiency and kinetics of CBZ were sharply decreased to 38.62% and $1.53 \times 10^{-2}$ $min^{-1}$, respectively, after adding 0.1 M EtOH into the binary CBZ-MNZ solution. A complete inhibition was obtained after the concentration of EtOH was increased to 1.0 M. This finding suggests the dominant role of $SO_4^{\bullet-}$ or $^{\bullet}OH$ in the degradation of CBZ. Relatively, the inhibition of TBA is much weaker than EtOH. For example, more than 98.84% of CBZ can still be removed in the presence of 1 M TBA within 45 min, which excludes the decisive role of $^{\bullet}OH$. Further increasing the concentration of TBA to 5 M can cause significant inhibition to the removal of CBZ (Fig. S6a, b). This is due to that the first-order reaction rate of 5 M TBA with $SO_4^{\bullet-}$ ($(2 – 4.05) \times 10^6$ $s^{-1}$) is comparable to that of 0.1 M EtOH ($(1.6 – 7.7) \times 10^6$ $s^{-1}$) [31], which can induce a comparable quenching effect caused by 0.1 M EtOH. The higher inhibition of 1 mM HD than that of 0.1 M EtOH implies that $^1O_2$ participated in the degradation of CBZ besides the decisive $SO_4^{\bullet-}$. The lower inhibition of BQ (1 mM) than HD (1 mM) implies the marginal role of $O_2^{\bullet-}$ in the degradation of CBZ. Additional quenching experiments in the single solution further verify the decisive role of $SO_4^{\bullet-}$ and the participation of $^1O_2$ in the degradation of CBZ (Fig. S7a, b).

**Table 1**
XPS fitting results on the Co 2p, O 1 s and Al 2p spectra of MCA before and after reaction.

| Samples | Co 2p (%) | | | | | O 1 s (%) | | | | | | Al 2p (%) | | |
|---|---|---|---|---|---|---|---|---|---|---|---|---|---|---|
| | $Co^{3+}$ | $Co^{2+}$ | $Co_{sat.}^{3+}$ | $Co_{sat.}^{2+}$ | $Co_{total}^{3+}/Co_{total}^{2+}$ | $O_{lat.}$ Co-O | Al-O | Total | $O_{Def.}$ | $O_{Surf.}$ | $O_{Def.}/O_{Lat.}$ | $Al_{Oh}^{3+}$ | $Al_{Td}^{3+}$ | $Al_{Oh}^{3+}/Al_{Td}^{3+}$ |
| Fresh MCA | 45.95 | 29.17 | 15.42 | 9.46 | 1.59 | 45.20 | 30.03 | 75.23 | 19.55 | 5.22 | 0.26 | 71.50 | 28.50 | 2.51 |
| Used in BZS | 36.66 | 40.48 | 14.03 | 8.83 | 1.03 | 18.22 | 38.77 | 56.99 | 35.75 | 7.26 | 0.63 | 41.80 | 58.20 | 0.72 |
| Used in SCS | 46.81 | 33.19 | 13.45 | 6.55 | 1.52 | 25.18 | 34.68 | 59.86 | 33.79 | 6.35 | 0.56 | 67.81 | 32.19 | 2.11 |
| Used in SMS | 43.17 | 38.21 | 12.58 | 6.04 | 1.26 | 20.63 | 38.60 | 59.23 | 33.49 | 7.28 | 0.57 | 47.03 | 52.97 | 0.89 |

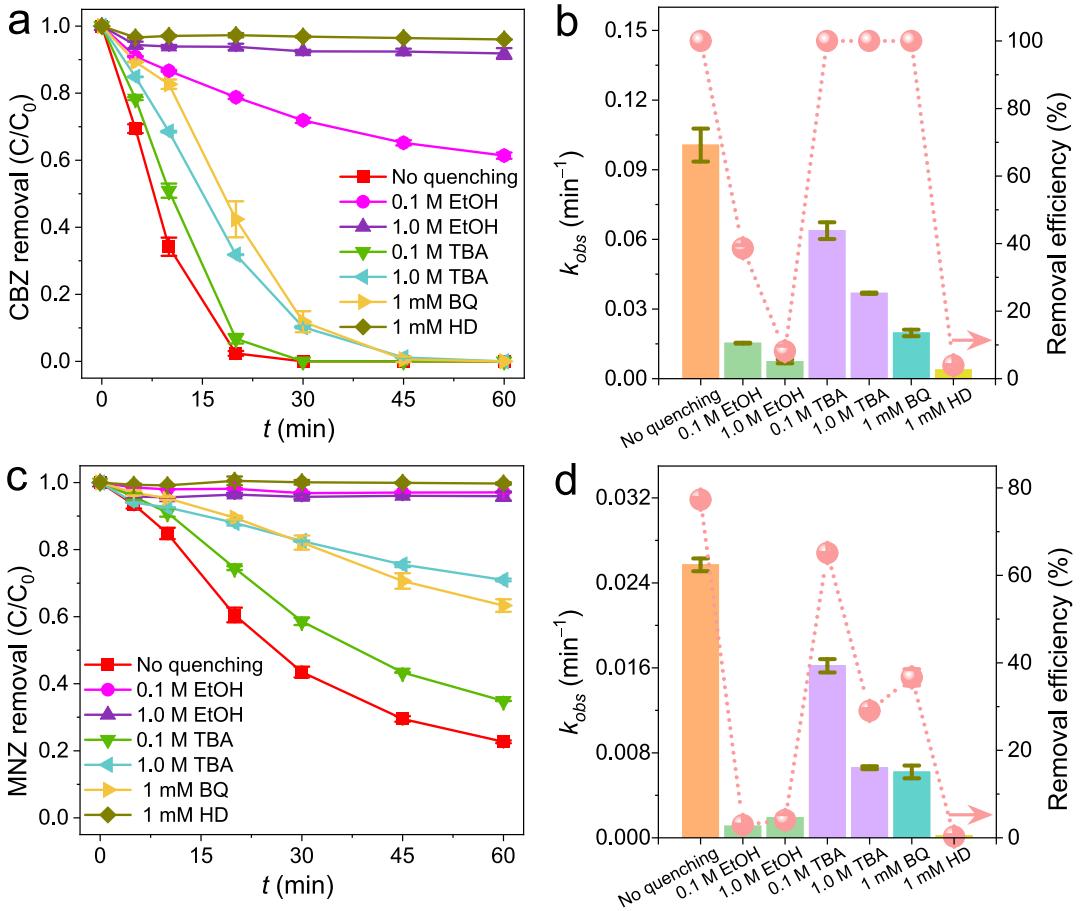


**Fig. 4.** Effects of various scavengers on the simultaneous removal of CBZ (a, b) and MNZ (c, d) from the binary CBZ-MNZ solution ([MCA] = 20 g/L, [CBZ] = [MNZ] = 10 mg/L, [PMS] = 1.0 mM, initial pH = 7.0, T = 25 ± 1 °C).

On the other hand, the presence of 0.1 M EtOH in the binary solution can completely inhibit the degradation of MNZ (Fig. 4c, d). This indicates the dominance of $SO_4^{\bullet-}$ and/or $^{\bullet}OH$ mediated radical oxidation process for the removal of MNZ. The lower inhibition of 1 M TBA than that of 0.1 M EtOH excludes the decisive role of $^{\bullet}OH$ in the oxidation degradation of MNZ. Under this case, the first-order reaction rate of 1 M TBA with $^{\bullet}OH$ ($(3.8 – 7.6) \times 10^8\ s^{-1}$) is two times higher than that of 0.1 M EtOH ($1.9 \times 10^8\ s^{-1}$) [31]. If $^{\bullet}OH$ was the decisive oxidant, in theory, 1 M TBA possesses higher inhibition to the removal of MNZ. However, the result was reverse. As mentioned above, the enhanced inhibition of TBA with the increased concentration is due to its increased quenching ability toward $SO_4^{\bullet-}$ (Fig. S6c, d). The remarkably decreased removal kinetics caused by HD and BQ is mainly due to their high second-order reaction rates with $SO_4^{\bullet-}$ ($10^8$ – $2.8 \times 10^9\ M^{-1}{\bullet}s^{-1}$) [31]. With the respect to the removal efficiency and kinetics of MNZ, the presence of 1 mM HD caused a comparable quenching effect compared with that of 0.1 M EtOH. This finding suggests the dominant role of $SO_4^{\bullet-}$ in the MNZ oxidation, but cannot completely exclude the formation of $^1O_2$. The insignificant of $O_2^{\bullet-}$ can be confirmed by the much lower inhibition of 1 mM BQ than 1 mM HD. The quenchers-regulated removal profiles of MNZ in the single solution further confirm that $SO_4^{\bullet-}$ was the primary radical responsible for the degradation of MNZ (Fig. S7c, d).

### 3.5.1. *Formation mechanism of ROS*

To probe the formation mechanism of ROS, we analyze the high resolution XPS spectra of Co 2p, Al 2p and O 1 s for MCA before and after use in the binary CBZ-MNZ solution (BZS), single CBZ solution (SCS), and single MNZ solution (SMS). It is clear that the Co $2p_{3/2}$ spectra of MCA can be well fit by four peaks at 779.70 eV ($Co^{3+}$), 781.10 eV ($Co^{2+}$), 784.40 eV (satellite of $Co^{3+}$, $Co_{sat.}^{3+}$) and 788.60 eV (satellite of $Co^{2+}$, $Co_{sat.}^{2+}$) (Fig. 5a, b and Fig. S8a, b) [48]. Obviously, Co elements within MCA exist in their oxidation forms of $Co^{2+}$ and $Co^{3+}$. The $Co^{3+}$ is usually coordinated at the octahedral ($O_h$) site (denoted as $Co_{Oh}^{3+}$) of MCA, while $Co^{2+}$ is usually at the tetrahedral ($T_d$) site (denoted as $Co_{Td}^{2+}$) [49]. For all the cases, the Al 2p spectra can be deconvoluted into two sub-peaks: the one for the binding energy of 73.50 eV is due to

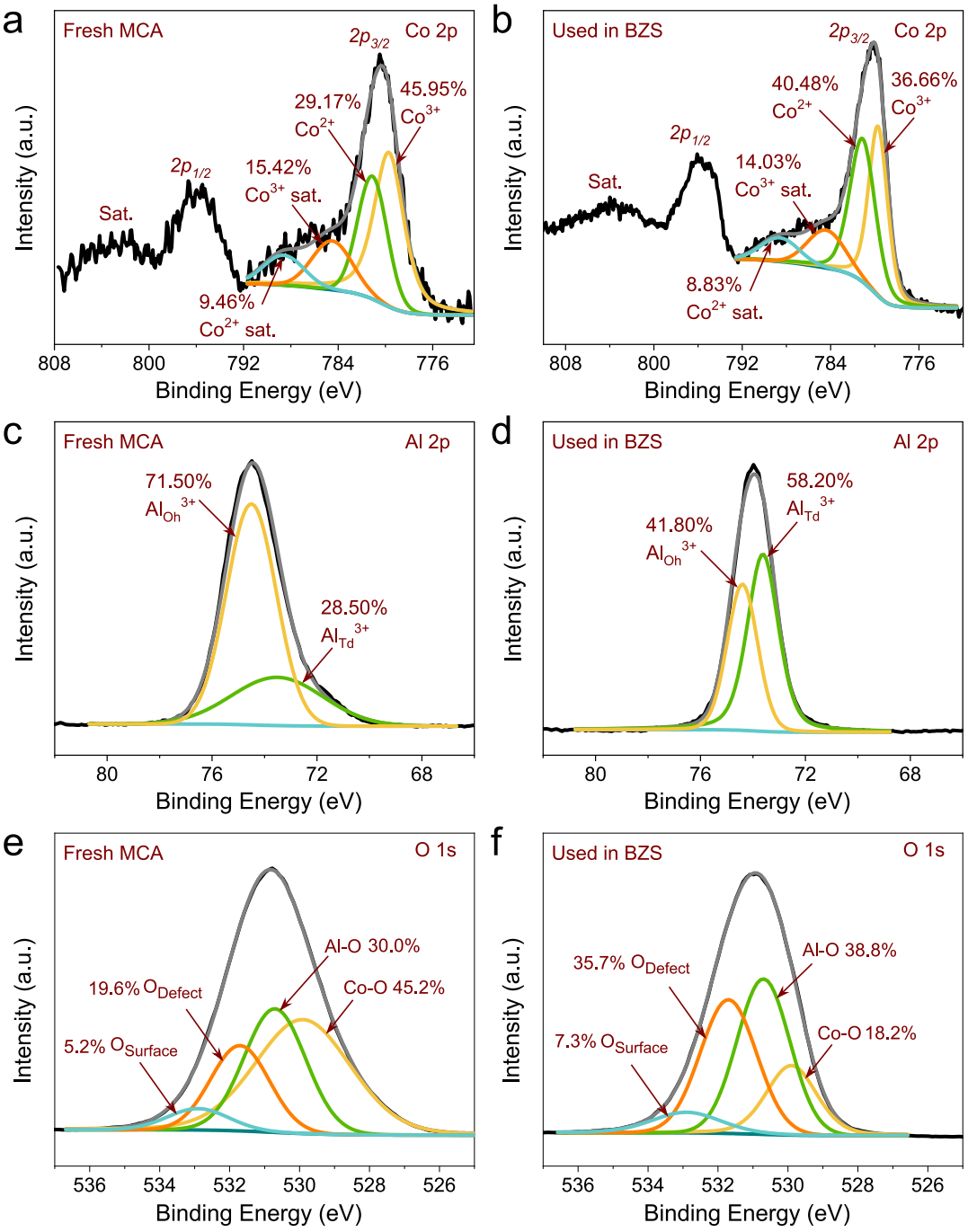


**Fig. 5.** XPS analysis for the Co 2p (a, b), O 1 s (c, d), and Al 2p (e, f) spectra of MCA before and after use in the binary CBZ-MNZ solution.

the $Al^{3+}$ coordinated at the $T_d$ site of $Co_2AlO_4$ (denoted as $Al_{Td}^{3+}$), while the other for the binding energy of 74.50 eV is ascribed to the $Al^{3+}$ at the $O_h$ site (denoted as $Al_{Oh}^{3+}$) (Fig. 5c, d and Fig. S8c, d) [50]. The O 1 s spectra can be well fitted with the Co-O band (529.90 eV), Al-O band (530.70 eV), defective oxygen (around 531.70 eV, denoted as $O_{Def.}$) and surface-adsorbed oxygen (around 532.90 eV, denoted as $O_{Sur.}$) (Fig. 5e, f and Fig. S8e, f) [23,51]. For the $Co_2AlO_4$ with normal spinel structure, the $Co^{3+}$ coordinated at the $O_h$ site is usually bonded with $Al_{Oh}^{3+}$ to form $Al_{Oh}^{3+}$-O-$Co_{Oh}^{3+}$, while the $Co^{2+}$ at the $T_d$ site prefers to bond with $Al_{Td}^{3+}$ (forming $Al_{Td}^{3+}$-O-$Co_{Td}^{2+}$) [49].

After used in the binary solution, the ratio of $Co_{total}^{3+}/Co_{total}^{2+}$ within MCA showed an obvious decrease (from 1.59 to 1.03, Table 1). This is due to the trade-off between the electron-withdrawing and/or-donating processes of interfacial $Co^{3+}/Co^{2+}$ species and PMS. Over the PMS activation by MCA, the transformation of $Co_{Td}^{2+}$ to $Co_{Oh}^{3+}$ can lead to the formation of $SO_4^{\bullet-}$ via the electron transfer from the $Co_{Td}^{2+}$ species of MCA to PMS (cf. Reaction 11); meanwhile, the electron transfer from PMS to the $Co_{Oh}^{3+}$ species of MCA can induce the formation of $SO_5^{\bullet-}$, which can be further converted into $^1O_2$ (see Reaction 12 – 13) [52]. The decreased ratio of $Co_{total}^{3+}/Co_{total}^{2+}$ suggests a favorable electron transfer from PMS to interfacial $Co_2AlO_4$ [29]. The quenching results further confirmed the formation of $SO_4^{\bullet-}$ and $^1O_2$ (cf. Fig. 4, Fig. S6 – S7). It is found that the Al species within MCA still exists in the forms of $Al^{3+}$, excluding its direct role in PMS activation. Nevertheless, the spatial positions of Al atoms varied greatly. For example, after activating PMS in the binary solution, the contents of

$Al_{Oh}^{3+}$ and $Al_{Td}^{3+}$ have changed from 71.50% and 28.50% to 41.80% and 58.20%, respectively (Table 1). We consider that this is due to the changes between $Co_{Td}^{2+}$ and $Co_{Oh}^{3+}$. As mentioned above, there exists a robust bond of Al-O-Co within MCA (i.e., $Al_{Oh}^{3+}$-O-$Co_{Oh}^{3+}$ and $Al_{Td}^{3+}$-O-$Co_{Td}^{2+}$). From the view of maintaining the spatial structure stability of interfacial $Co_2AlO_4$, it is easy to understand that decreasing the content of $Co_{Oh}^{3+}$ inevitably resulted in the low content of $Al_{Oh}^{3+}$, and increasing the content of $Co_{Td}^{2+}$ increased the content of $Al_{Td}^{3+}$. The flexible changes of Al atoms between the octahedral and tetrahedral sites are favorable for the transformation of $Co_{Td}^{2+}$ to $Co_{Oh}^{3+}$ or $Co_{Oh}^{3+}$ to $Co_{Td}^{2+}$, thus promoting PMS decomposition and ROS formation. Although the oxygen vacancy (or defective oxygen) has been considered as a force for PMS activation [53–55], the increased content of $O_{Def.}$ (from 19.55% to 35.75%, Table 1) for the MCA sample used in the binary solution excludes such role. The content of lattice oxygen (including Co-O and Al-O) has been decreased from 75.23% to 56.99%. We think that this is ascribed to the synergistic interactions between Al and Co atoms within $Co_2AlO_4$ for maintaining the stability of the spinel structure over PMS activation.

It is clear that the ratio of $Co_{total}^{3+}/Co_{total}^{2+}$ for MCA used in the binary solution is much lower than those of MCA samples used in the single CBZ or MNZ solution (Table 1). The enhanced progression of Al-O-Co bond from $Al_{Oh}^{3+}$-O-$Co_{Oh}^{3+}$ to $Al_{Td}^{3+}$-O-$Co_{Td}^{2+}$ probably attributes to this phenomenon. In theory, the co-presence of CBZ and MNZ would consume more ROS to realize their oxidation degradation, which relies on the transformation rate of $Co_{Td}^{2+}$ to $Co_{Oh}^{3+}$ or $Co_{Oh}^{3+}$ to $Co_{Td}^{2+}$ (cf. Reaction 11 – 12). Interestingly, the ratios of $Co_{total}^{3+}/Co_{total}^{2+}$ are highly linear with the contents of $Al_{Oh}^{3+}$ and the ratios of $Al_{Oh}^{3+}/Al_{Td}^{3+}$ for fresh or used MCA samples (Table 1, Fig. S9). This further confirms the synergistic role of Al and Co atoms in the PMS activation and the stability of the spinel structure for $Co_2AlO_4$.

$$Co^{2+} + HSO_5^- \rightarrow Co^{3+} + SO_4^{\bullet-} + OH^- \quad (11)$$

$$Co^{3+} + HSO_5^- \rightarrow Co^{2+} + SO_5^{\bullet-} + H_2O \quad (12)$$

$$2SO_5^{\bullet-} + H_2O \rightarrow 2HSO_4^- + 1.5\ {}^1O_2 \quad (13)$$

### 3.5.2. ROS-regulated degradation of CBZ and MNZ

The simultaneous and single removal mechanism of CBZ and MNZ by MCA/PMS is proposed in Fig. 6. As mentioned above, the interfacial $Co^{3+}/Co^{2+}$ species is rich in $Co_2AlO_4@Al_2O_3$. The presence of Al atoms enables the robust bond of Al-O-Co to form a special $Co_2AlO_4$ spinel structure on $Al_2O_3$, thus endowing a flexibility in transformation of $Co_{Td}^{2+}$ to $Co_{Oh}^{3+}$ or $Co_{Oh}^{3+}$ to $Co_{Td}^{2+}$ for the PMS activation and ROS formation (*via* Reaction 11 – 13). Compared with the single removal process, the ratio of $Co_{total}^{3+}/Co_{total}^{2+}$ for MCA was remarkably decreased after activating PMS in the binary CBZ-MNZ solution (Table 1). Whether MCA used in the binary or single solution, a good linear relationship is obtained between the ratios of $Co_{total}^{3+}/Co_{total}^{2+}$ and the contents of $Al_{Oh}^{3+}$ (or the ratios of $Al_{Oh}^{3+}/Al_{Td}^{3+}$) (Fig. S9), suggesting the combined role of Al and Co atoms in the PMS activation for the removal of CBZ and MNZ. In general, the interfacial $Co_2AlO_4$ on MCA activated PMS to generate the dominant oxidants of $SO_4^{\bullet-}$ and $^1O_2$ simultaneously for the degradation of CBZ and MNZ. Since the electron donating ability of $-CONH_2$ group within CBZ is stronger than that of $-NO_2$ group within MNZ, $SO_4^{\bullet-}$ prefers to attack the CBZ molecules rather than MNZ in the binary solution of CBZ and MNZ [39]. Meanwhile, the highly selective oxidant of $^1O_2$ with robust anti-interference capacity is inclined to attack the CBZ molecules but inert to MNZ [40,41]. From the view of electrostatic interaction, the positive CBZ ($pK_a$ = 13.94) is easier to be attacked by $SO_4^{\bullet-}$ compared with the negative MNZ ($pK_{a1}$ = 2.40) [33,34], although the second order reaction rate constant of MNZ with $SO_4^{\bullet-}$ is higher than CBZ ($2.74 \times 10^9\ M^{-1}\cdot s^{-1}$ versus $1.92 \times 10^9\ M^{-1}\cdot s^{-1}$) [37]. All these reasons explain the phenomenon why the removal of CBZ was slightly inhibited in the binary system compared with the single system (Figs. 1 – 2).

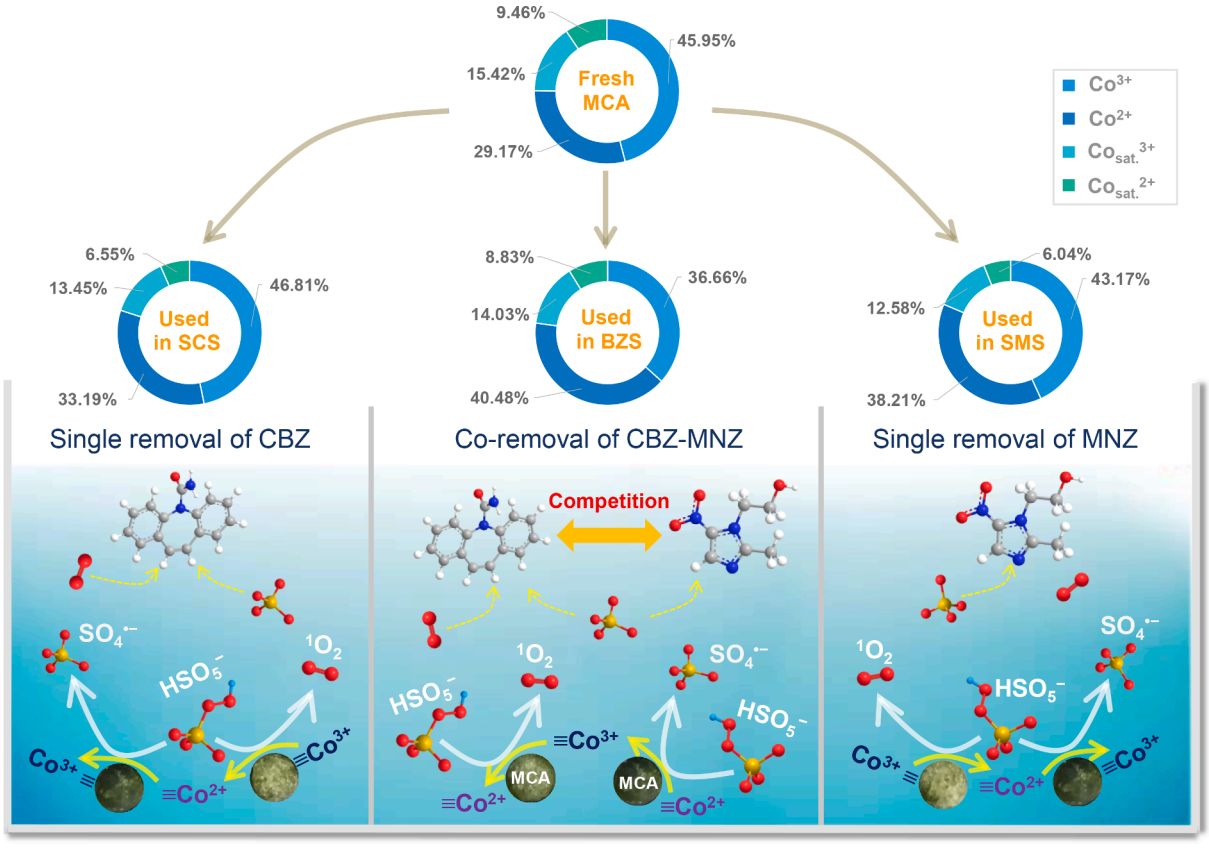


**Fig. 6.** The proposed removal mechanisms of CBZ and MNZ by PMS/MCA.

### 3.6. Pathways for the degradation of CBZ and MNZ

The transformation products of CBZ and MNZ were identified by HPLC/MS/MS (Fig. S10 – S12, Table S2 – S4). Fig. 7 demonstrates varied product distributions for singly and simultaneously degrading CBZ and MNZ by the $Co_2AlO_4$@APs/PMS system. Ten oxidation products of CBZ were formed in the binary solution of CBZ and MNZ, while in the single CBZ solution, twelve products were detected. Interestingly, whether in the single solution of CBZ or the binary solution of CBZ and MNZ, the product with *m/z* of 253 [+MS model] (more than 71%) was found as the primary product for the degradation of CBZ. Other transformation products, i.e., C266-10.5, C270-9.5, C282-10.2, C146-7.2, C137-9.2, C165-12.6 and C162-8.1, were formed in the binary CBZ-MNZ solution and the single CBZ solution, but different in their contents. C179-8.6 and C270-9.4 were only generated in the binary CBZ-MNZ solution, while the transformation products only found in the single CBZ solution were C250-10.0, C266-9.9, C195-10.7, C286-9.1 and C286-8.7. Besides four transformation products formed in the binary solution, more than 85% of MNZ was not degraded due to the coexistence of CBZ. In the absence of CBZ, MNZ was completely oxidized with M103-1.8 (56.9%) and M102-1.6 (40.1%) being as the primary products. The significant changes on the transformation products of MNZ suggest that the co-degradation behaviors of CBZ and MNZ are quite different from their single ones.

As mentioned earlier, $SO_4^{\bullet-}$ and $^1O_2$ were formed in the MCA/PMS system responsible for the oxidation degradation of CBZ and MNZ. For the degradation of CBZ, it was reported that the olefinic double bond of central heterocyclic ring (at the C7 and C7′ sites of CBZ, Fig. 8a) can be easily attacked by ROS [44,56,57]. For the degradation of CBZ by $SO_4^{\bullet-}$, the single electron transfer (SET) reaction is more thermodynamically favorable than radical addition and H-abstraction [56]. Therefore, we think that the initial step was the attack of $SO_4^{\bullet-}$ on the olefinic double bond of CBZ, resulting in a transition species (TS1) with a *m/z* of 234 via the abstraction of two electrons. The oxygen addition on TS1 leads to C252-10.4. The contents of C252-10.4 in the binary and single solutions are 74.98% and 71.51%, respectively (Fig. 7a, c). The high content of C252-10.3 suggests that the SET was the dominated pathway for the degradation of CBZ. Although the shared primary pathway in the single and binary solutions can make the removal kinetics of CBZ less vulnerable to the interference of MNZ, the differences on the product distributions and transformation pathways of CBZ still exist. For instance, the second most important product for the degradation of CBZ in the binary solution is C179-8.6 (10.38%), while the second one in the single solution is the product of C266-10.5 (6.96%). These two products can be evolved from TS1 via different reaction pathways. For the formation of C179-8.6, the involved steps are: the C–C cleavage of TS1 to form the transition species of TS2, the arrangement of TS2 to form the transition species of TS3, the N-C cleavage and aldehyde oxidation of TS3 to form the transition species of TS4, and the decarboxylation of TS4. For the formation of C266-10.5, the electron abstraction from TS1 was firstly initiated by $SO_4^{\bullet-}$ to form the transition species of TS5, and then the N-C coupling occurred intramolecularly for TS5 to generate C266-10.5.

The pathways of subordinate products for the degradation of CBZ in the binary solution were summarized as follows: The hydrolysis of TS1 and the followed oxygen addition led to C270-9.4 [58], while the combined reactions of hydrolysis, oxygen addition and electron abstraction occurred on TS1 induced the formation of TS6. The resultant TS6 was further converted into C266-9.9 via the N-C coupling, which was further transferred into C282-10.2 via electron abstraction, hydrolysis and oxygen addition. The C195-10.7 was formed via the reactions of N-C cleavage, aldehyde oxidation and decarboxylation of TS3. The abstraction of two electrons at the C1 and C7 sites (or the C1′ and C7′ sites) of CBZ resulted in the transition species of TS7, which was converted into C270-9.5 via the reactions of hydrolysis and oxygen addition. The resultant C270-9.4 and C270-9.5 were converted into C286-8.7 and C286-9.1, respectively, via the reactions of electron abstraction, hydrolysis and oxygen addition. The N-C cleavage of TS2 induced the formation of the transition species of TS8, which was then evolved into C137-9.2, C146-7.1, C162-8.1 or C166-12.6 via the aldehyde oxidation, deaminization, hydrolysis and/or intramolecular ring formation. Noted that C266-9.9 resulted from the aldehyde oxidation for TS6 can only be formed in the single CBZ solution. Compared with the degradation of CBZ in the binary CBZ-MNZ solution, C286-9.1 and C286-8.7 in the

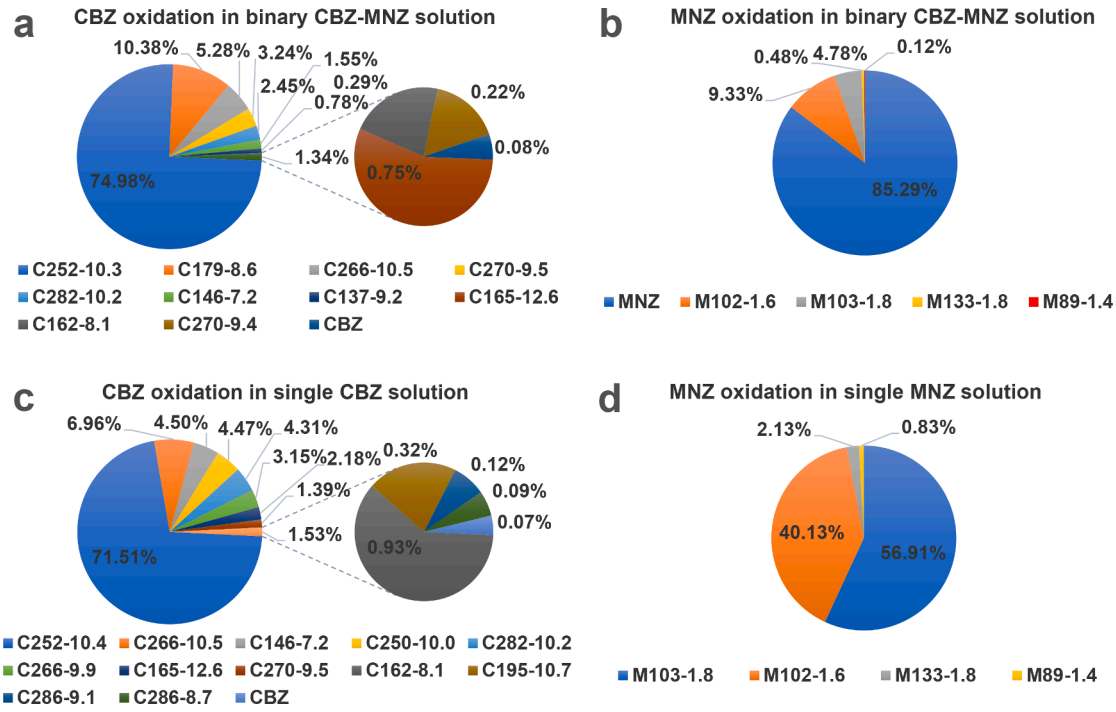


**Fig. 7.** Product distribution for the degradation of CBZ and/or MNZ by MCA/PMS in the binary CBZ-MNZ solution (a, b), single CBZ solution (c) and single MNZ solution (d).

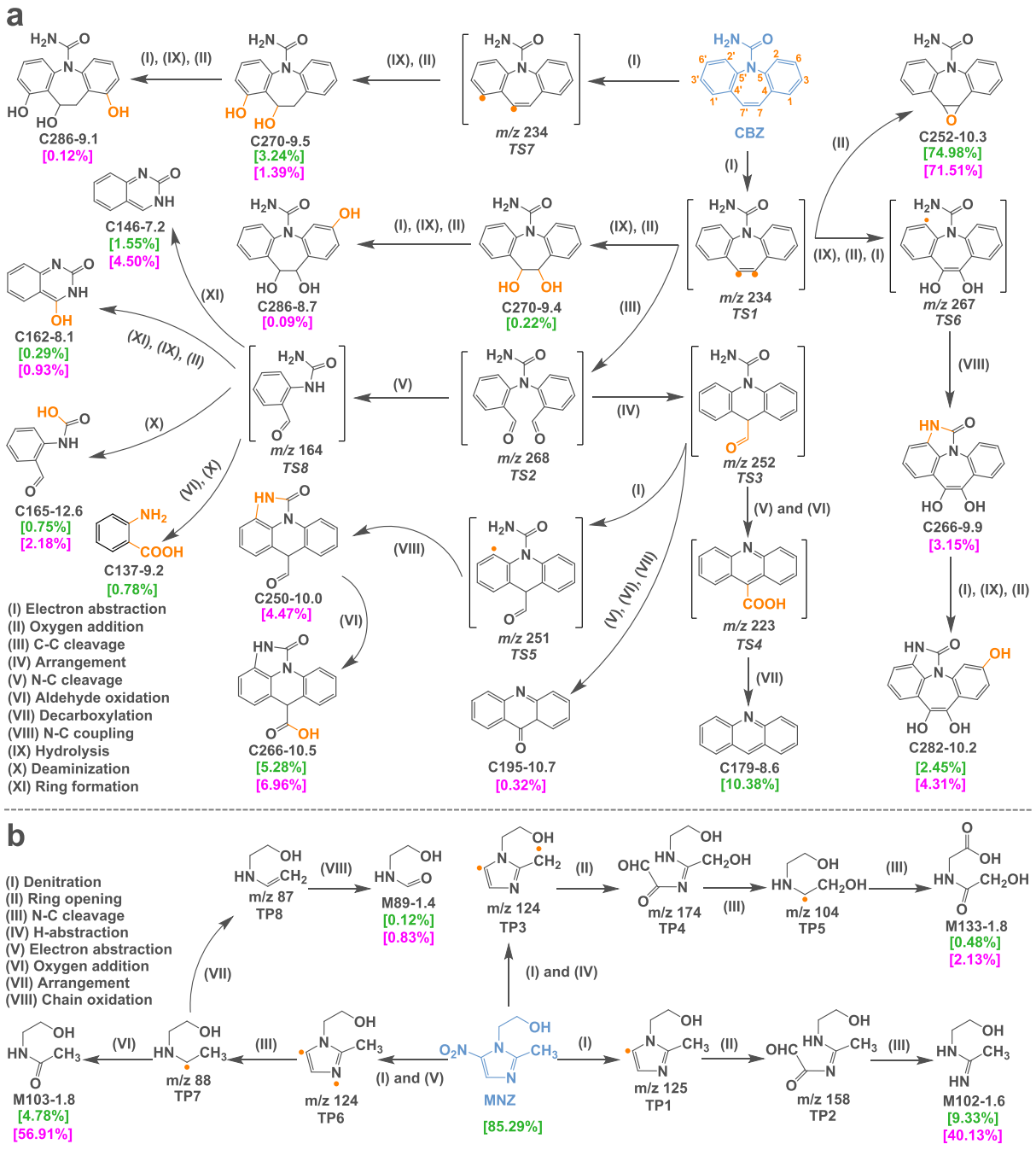


**Fig. 8.** Proposed oxidation pathways of CBZ (a) and MNZ (b) by MCA/PMS in the binary CBZ-MNZ solution and the single CBZ (or MNZ) solution. The green and lavender data in the brackets represents the ratios of products formed in the binary and single solutions, respectively.

single CBZ solution were also resulted from the deep oxidation of C270-9.5 and C270-9.4, respectively. These observations reveal different transformation pathways in the single CBZ and binary CBZ-MNZ solutions, clearly suggesting the competition reactions between CBZ and MNZ over their degradation by the MCA/PMS system. In general, the presence of MNZ showed a slight disturbance on the formation of first priority transformation products and the oxidation kinetics for the removal of CBZ.

For the degradation of MNZ (shown in Fig. 8b), the denitration of $-NO_2$ group from MNZ was the first step to form a transition product of TP1 caused by the attack of $SO_4^{\bullet-}$. The followed step was the imidazole ring opening of TP1 to form another transition product of TP2, which was ultimately converted into M102-1.6 via the N-C cleavage. The attack of $SO_4^{\bullet-}$ on MNZ also resulted in a transition product of TP3 (a dual-carbon-centered radical product) via an integrated pathway of denitration and H-abstraction. The imidazole ring opening of TP3 (to form TP4) and the followed cleavage of N-C double bond of TP4 (to form another radical transition product of TP5) were two necessary steps for the formation of M133-1.8. Meanwhile, a nitrogen-carbon-centered radical product, i.e., TP6, was formed caused by the attack of $SO_4^{\bullet-}$ on the imidazole ring of MNZ. The transition product of TP7 can be generated via the integrated N-C and N = C cleavage. The oxygen addition on TP7 contributed to the formation of M103-1.8. On the other hand, the arrangement of TP7 induced the formation of an olefin-based transition product of TP8, which was further converted into M89-1.4 via the chain oxidation. Although the aforementioned pathways were

involved in the degradation of MNZ in the binary CBZ-MNZ solution, 85.29% of MNZ was still retained (Fig. 7b). By contrast, in the absence of CBZ, MNZ can be completely degraded with M103-1.8 (56.91%) and M102-1.6 (40.13%) as the primary products. These findings indicate that CBZ in the binary solution remarkably altered the degradation behaviors of MNZ by the $Co_2AlO_4$@APs/PMS system.

### 3.7. Toxicity evaluation

The T.E.S.T software was employed to predict the toxicity of the degradation products to comparably evaluate their ecosystem risks regarding the removal of CBZ and MNZ by the MCA/PMS system. Figs. 9 – 10 and Table S5 – S7 show the predicted toxicity indicators, i.e., bioaccumulation factor (BAF), development toxicity, mutagenicity, and acute toxicity (LC50 and LD50) for each product. Based on the product distributions/ratios, normalized toxicity indicators had also been provided to assess the overall toxicity of the oxidation products of CBZ (or MNZ) in the binary or single solution [31]. Besides C179-8.6 (in the binary solution, 116.25), C195-10.7 (in the single solution, 48.55) and C282-10.2 (27.55), the rest of the products have lower BAF values than that of parent CBZ (26.63) (Fig. 9a). Compared with the parent CBZ (or MNZ), the normalized total BAF value of the products for the individual removal of CBZ (or MNZ) was decreased; while the oxidation products of CBZ (or MNZ) in the binary CBZ-MNZ solution have a higher total BAF

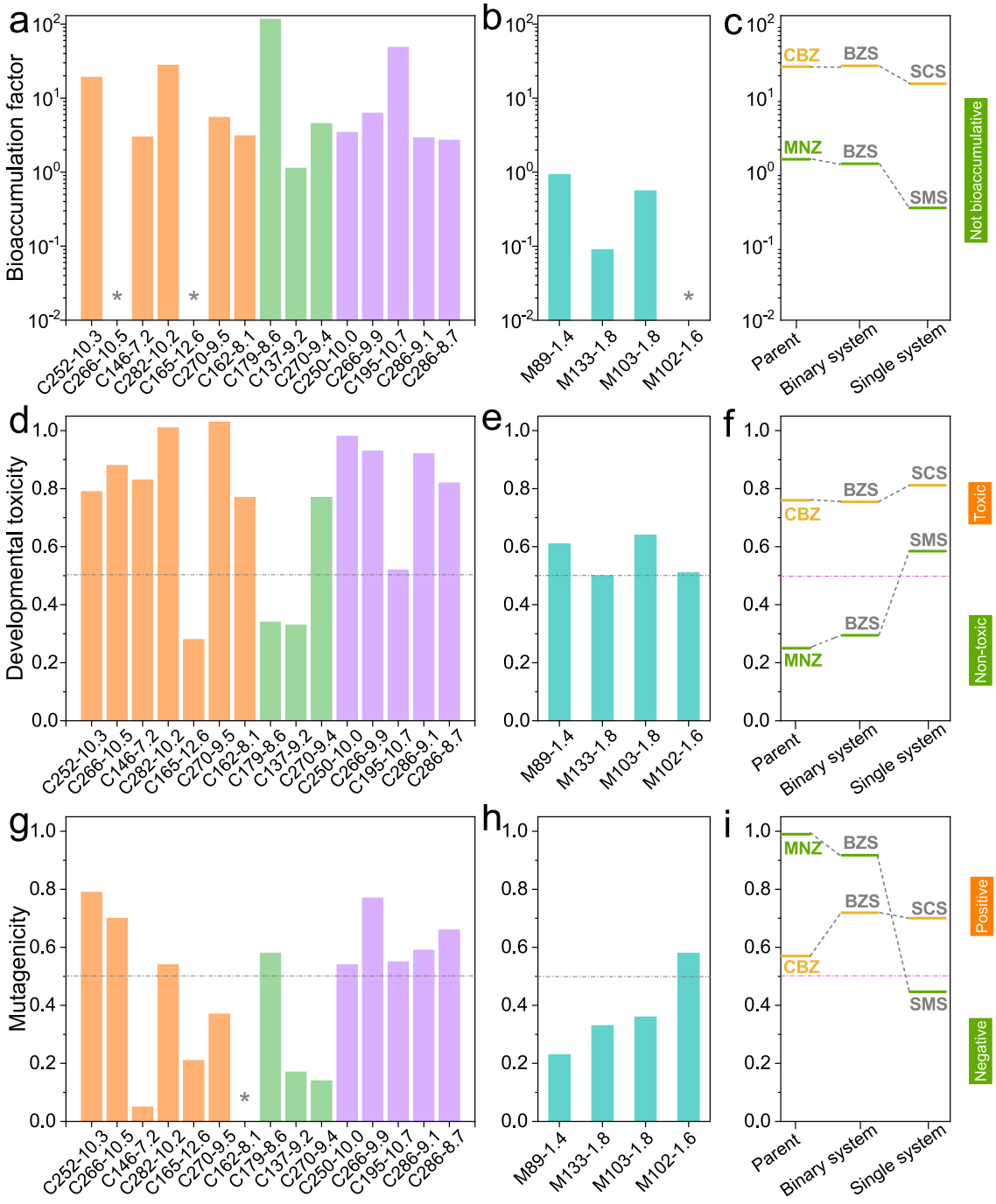


**Fig. 9.** The predicted bioaccumulation factor (a, b), developmental toxicity (d, e), and mutagenicity (g, h) of parent CBZ (or MNZ) and their oxidation products, as well as the normalized total bioaccumulation factor (c), developmental toxicity (f), and mutagenicity (i) for all the products of CBZ (or MNZ) in the binary and single solution. * means the data are not available.

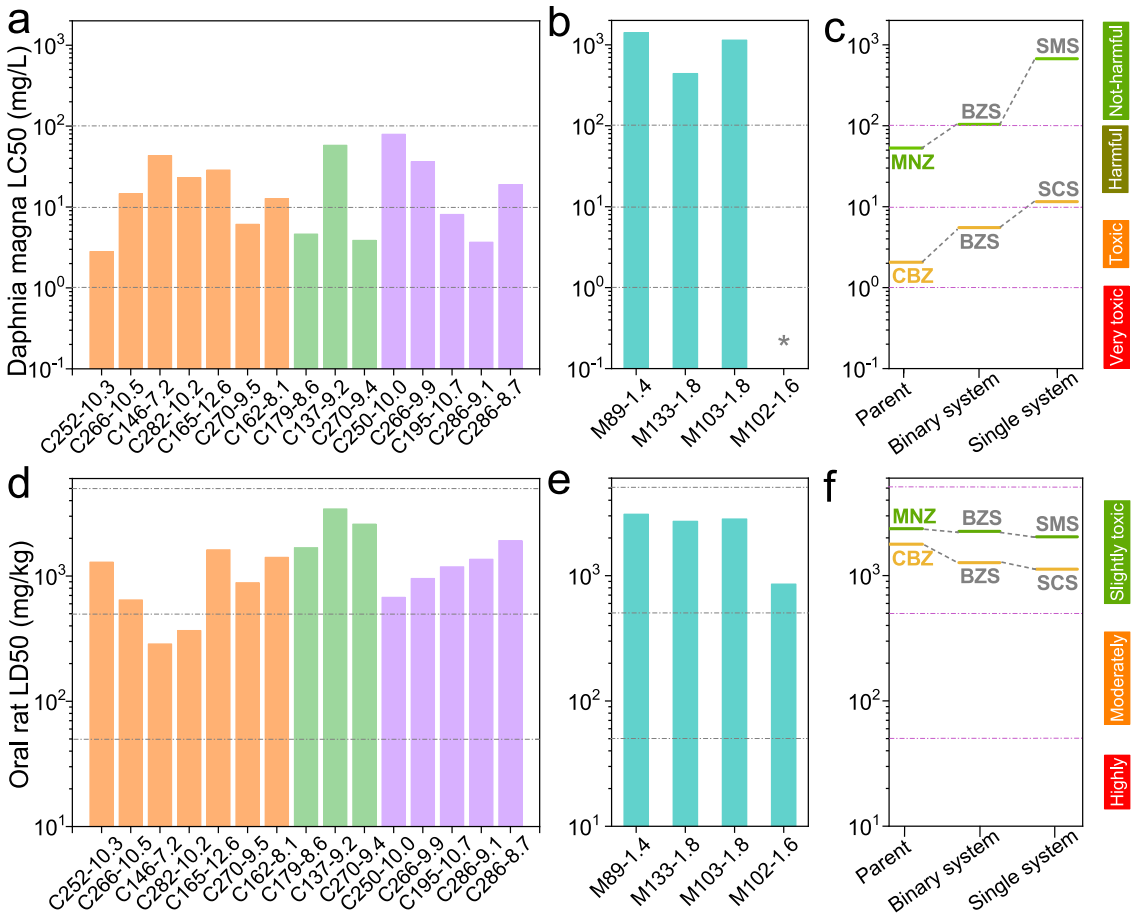


**Fig. 10.** The acute toxicity, *Daphnia magna* LC50 (a, b) and *Oral rat* LD50 (d, e) of parent CBZ (or MNZ) and their oxidation products, as well as the normalized total LC50 (c) and LD50 (f) for all the products of CBZ (or MNZ) in the binary and single solution. * means the data are not available.

value than that of the products in the single CBZ (or MNZ) solution (Fig. 9b, c, Table S8). This finding suggests that the co-existence of CBZ and MNZ increased the bioaccumulation potential of the degradation products. Despite the above changes on the BAF values for the co-removal of CBZ and MNZ, the bioaccumulation potentials of CBZ, MNZ and their degradation products in fish can be neglected based on the U.S. Environmental Protection Agency's regulation [59].

Obviously, the parent CBZ (0.76) is a developmental toxicant, while the parent MNZ (0.25) is a developmental non-toxicant (Fig. 9d, e). For the degradation products of CBZ in the binary CBZ-MNZ solution, C179-8.6, C137-9.2 and C165-12.6 are not developmentally toxic, while for the single CBZ solution, only C165-12.6 is the developmental non-toxicant. Besides M133-1.8 formed in the binary solution, M89-1.4, M102-1.6 and M103-1.8 are developmental toxicants. The analysis on the normalized total developmental toxicity indicates that the degradation products of CBZ either in the binary or the single solution are developmental toxic (Fig. 9f, Table S8). For the degradation products of MNZ formed in the binary CBZ-MNZ solution or the single MNZ solution, they have higher normalized total developmental toxicity values than the parent MNZ. Although the degradation products formed in the single CBZ (or MNZ) solution have higher normalized total developmental toxicity than the parent CBZ (or MNZ), the degradation products of CBZ (or MNZ) in the binary CBZ-MNZ solution possess lower normalized total developmental toxicity than those in the single CBZ (or MNZ) solution (Fig. 9f, Table S8). This implies that the co-existence of CBZ and MNZ helps to reduce the developmental toxicity of the degradation products.

As shown in Fig. 9g, h, CBZ (0.57) and MNZ (0.99) are mutagenic pollutants because their predicted mutagenicity values are above 0.5. The mutagenic products for the degradation of CBZ in the binary CBZ-MNZ and single CBZ solutions are C252-10.3, C266-10.5, C282-10.2, C179-8.6, C250-10.0, C266-9.9, C195-10.7, C286-9.1 and C286-8.7. Despite the reduced number of mutagenic products in the binary CBZ-MNZ solution, the presence of MNZ increased the total mutagenicity value of the degradation products of CBZ compared with the products in the single CBZ solution. In addition, the degradation products of CBZ (either in the binary CBZ-MNZ or the single CBZ solution) have higher normalized total mutagenicity values than parent CBZ (Fig. 9i, Table S8). Even though the degradation products of MNZ in the binary CBZ-MNZ solution have higher normalized total mutagenicity value than those in the single MNZ solution, the degradation products of MNZ in the binary CBZ-MNZ or single MNZ solution have lower individual and normalized total mutagenicity values than parent MNZ (Fig. 9i, Table S8). These findings indicate that the co-removal of CBZ and MNZ by the MCA/PMS system shows more mutagenicity risk than individual removal.

Based on the predicted LC50 values, CBZ (2.06 mg/L) is toxic to *Daphnia magna* (1 – 10 mg/L) while MNZ (53.09 mg/L) is harmful to *Daphnia magna* (10 – 100 mg/L) (Fig. 10a, b) [60]. It is clear that all the products for the degradation of CBZ under the binary or single condition have higher LC50 values than parent CBZ (Fig. 10c, Table S5 – S6). However, four products in the binary CBZ-MNZ solution (C252-10.3, C270-9.5, C179-8.6 and C270-9.4) and four products in the single CBZ solution (C252-10.3, C270-9.5, C195-10.7 and C286-9.1) are still found to be toxic to *Daphnia magna*. As shown in Fig. 10c and Table S8, the total LC50 values for the degradation products of CBZ in the single and binary systems are higher than parent CBZ. The normalized total LC50 value for the binary solution (5.52 mg/L) is lower than that for the single

solution (11.54 mg/L). These findings suggest that the presence of MNZ exerts a slight adverse effect on reducing the toxicity to *Daphnia magna* for the degradation of CBZ by MCA/PMS. Whether MNZ was degraded in the single or binary solution, all the products have much higher LC50 values (greater than442 mg/L) than parent MNZ (53.09 mg/L) (Fig. 10b, Table S7). The total LC50 value for the oxidation products in the single solution is much higher than that of binary solution (672.43 vs 103.84 mg/L) (Fig. 10c, Table S8). This finding implies that CBZ in the binary CBZ-MNZ solution significantly impaired the ability of MCA/PMS to lower the toxicity to *Daphnia magna* for the degradation of MNZ.

The *Oral rat* LD50 values of CBZ and MNZ were predicted as 1783.10 and 2371.74 mg/kg, respectively, indicating that they are slightly toxic to *Oral rat*. The higher the LD50 value is, the lower the toxicity is. Besides C137-9.2 (3432.75 mg/kg), C270-9.4 (2597.12 mg/kg), and C286-8.7 (1918.20 mg/kg), the rest of products in the single or binary solution have lower LD50 values than parent CBZ (Fig. 10d, Table S6), while for the removal of MNZ, only M102-1.6 (857.76 mg/kg) shows lower LD50 value than parent MNZ (Fig. 10e, Table S7). The total LD50 values for the degradation products of CBZ (or MNZ) in the single and binary solutions are lower than parent CBZ (or parent MNZ) (Fig. 10f, Table S8). These results imply that the removal of CBZ and MNZ by MCA/PMS increased their acute toxicity risk to rat. Interestingly, the oxidation products formed in the binary CBZ-MNZ solution have lower total LD50 values than the products in their single solution (Fig. 10f). This is due to the fact that there exists high proportion of products with less toxicity to rate formed in the binary solution (cf. Fig. 7, Table S5 – S7). Despite the above changes on the LD50 values, the oxidation products of CBZ and MNZ by MCA/PMS present slight acute toxicity to rat.

## 4. Conclusions

In summary, we systematically evaluated the efficacy of $Co_2AlO_4$@$Al_2O_3$ millispheres toward catalytically removing CBZ and MNZ simultaneously. The dominant oxidants in the monolithic $Co_2AlO_4$@$Al_2O_3$/PMS oxidation system are $SO_4^{\bullet-}$ and $^1O_2$. Because of the higher oxidation affinity of $SO_4^{\bullet-}$ and $^1O_2$ toward CBZ, the reduced ratio for the removal kinetics of CBZ was less than 35.41%, while that for the removal of MNZ reached 72.16%. $Cl^-$, $HCO_3^-$ and $PO_4^{3-}$ caused distinctive inhibition to the removal of CBZ and MNZ (besides the enhanced removal of CBZ by $Cl^-$). Compared with the single removal process, the simultaneous oxidation process remarkably changed the distributions of the products of CBZ and MNZ. The simultaneous removal process generally increased the total bioaccumulation potential and mutagenicity risk of the degradation products, but helped to reduce their total developmental toxicity. The products in the binary solution showed higher total acute toxicity to *Daphnia magna* than those of the single solution, while for the total acute toxicity to *Oral rat*, the results were just the opposite. This work suggests the necessity of comprehensively studying the monolithic catalysts-oriented AOP toward the simultaneous removal of multiple emerging contaminants for water purification/detoxification.

### *CRediT authorship contribution statement*

**Min-Ping Zhu:** Conceptualization, Methodology, Investigation, Formal analysis, Visualization, Writing – original draft. **Jia-Cheng E. Yang:** Conceptualization, Methodology, Supervision, Visualization, Writing – review & editing, Funding acquisition. **Darren Delai Sun:** Writing – review & editing. **Baoling Yuan:** Writing – review & editing. **Ming-Lai Fu:** Supervision, Resources, Writing – review & editing, Funding acquisition.

### Declaration of Competing Interest

The authors declare that they have no known competing financial interests or personal relationships that could have appeared to influence the work reported in this paper.

### Acknowledgements

This work was partially supported by National Natural Science Foundation of China (Grant Nos. 51978638 and 51808524), Natural Science Foundation of Fujian Province (Grant No. 2020 J01120) and Scientific Research Funds of Huaqiao University (20BS109).

### Appendix A. Supplementary data

Supplementary data to this article can be found online at https://doi.org/10.1016/j.cej.2022.135201.

### References

[1] M. Patel, R. Kumar, K. Kishor, T. Mlsna, C.U. Pittman, D. Mohan, Pharmaceuticals of Emerging concern in aquatic systems: chemistry, occurrence, effects, and removal methods, Chem. Rev. 119 (2019) 3510–3673.
[2] N. Liu, X. Jin, C. Feng, Z. Wang, F. Wu, A.C. Johnson, H. Xiao, H. Hollert, J. P. Giesy, Ecological risk assessment of fifty pharmaceuticals and personal care products (PPCPs) in Chinese surface waters: a proposed multiple-level system, Environ. Int. 136 (2020), 105454.
[3] X. Yu, Q. Sui, S. Lyu, W. Zhao, J. Liu, Z. Cai, G. Yu, D. Barcelo, Municipal solid waste landfills: an underestimated source of pharmaceutical and personal care products in the water environment, Environ. Sci. Technol. 54 (2020) 9757–9768.
[4] J. Kang, H. Zhang, X. Duan, H. Sun, X. Tan, S. Liu, S. Wang, Magnetic Ni-Co alloy encapsulated N-doped carbon nanotubes for catalytic membrane degradation of emerging contaminants, Chem. Eng. J. 362 (2019) 251–261.
[5] P.Y. Nguyen, G. Carvalho, M.A.M. Reis, A. Oehmen, A review of the biotransformations of priority pharmaceuticals in biological wastewater treatment processes, Water Res. 188 (2021), 116446.
[6] H. Zhi, D.W. Kolpin, R.D. Klaper, L.R. Iwanowicz, S.M. Meppelink, G.H. LeFevre, Occurrence and spatiotemporal dynamics of pharmaceuticals in a temperate-region wastewater effluent-dominated stream: variable inputs and differential attenuation yield evolving complex exposure mixtures, Environ. Sci. Technol. 54 (2020) 12967–12978.
[7] A. Rao, A. Kumar, R. Dhodapkar, S. Pal, Adsorption of five emerging contaminants on activated carbon from aqueous medium: kinetic characteristics and computational modeling for plausible mechanism, Environ. Sci. Pollut. R. 28 (2021) 21347–21358.
[8] W. Tian, J. Lin, H. Zhang, X. Duan, H. Wang, H. Sun, S. Wang, Kinetics and mechanism of synergistic adsorption and persulfate activation by N-doped porous carbon for antibiotics removals in single and binary solutions, J. Hazard. Mater. 423 (2022), 127083.
[9] Y.u. Lei, S. Cheng, N.a. Luo, X. Yang, T. An, Rate constants and mechanisms of the reactions of $Cl^{\bullet}$ and $Cl_2^{\bullet-}$ with trace organic contaminants, Environ. Sci. Technol. 53 (19) (2019) 11170–11182.
[10] S. Cheng, X. Zhang, X. Yang, C. Shang, W. Song, J. Fang, Y. Pan, The multiple role of bromide ion in PPCPs degradation under UV/chlorine treatment, Environ. Sci. Technol. 52 (4) (2018) 1806–1816.
[11] S. Luo, Z. Wei, R. Spinney, F.A. Villamena, D.D. Dionysiou, D. Chen, C.-J. Tang, L. Chai, R. Xiao, Quantitative structure–activity relationships for reactivities of sulfate and hydroxyl radicals with aromatic contaminants through single–electron transfer pathway, J. Hazard. Mater. 344 (2018) 1165–1173.
[12] Y. Huang, M. Kong, D. Westerman, E.G. Xu, S. Coffin, K.H. Cochran, Y. Liu, S. D. Richardson, D. Schlenk, D.D. Dionysiou, Effects of $HCO_3^-$ on degradation of toxic contaminants of emerging concern by UV/$NO_3^-$, Environ. Sci. Technol. 52 (21) (2018) 12697–12707.
[13] J. Wang, S. Wang, Reactive species in advanced oxidation processes: Formation, identification and reaction mechanism, Chem. Eng. J. 401 (2020), 126158.
[14] X. Liu, Y. Liu, S. Lu, Z. Wang, Y. Wang, G. Zhang, X. Guo, W. Guo, T. Zhang, B. Xi, Degradation difference of ofloxacin and levofloxacin by UV/$H_2O_2$ and UV/PS (persulfate): Efficiency, factors and mechanism, Chem. Eng. J. 385 (2020), 123987.
[15] S. Xiao, M. Cheng, H. Zhong, Z. Liu, Y. Liu, X. Yang, Q. Liang, Iron-mediated activation of persulfate and peroxymonosulfate in both homogeneous and heterogeneous ways: a review, Chem. Eng. J. 384 (2020), 123265.
[16] Z. Wu, Y. Wang, Z. Xiong, Z. Ao, S. Pu, G. Yao, B. Lai, Core-shell magnetic $Fe_3O_4$@Zn/Co-ZIFs to activate peroxymonosulfate for highly efficient degradation of carbamazepine, Appl. Catal. B Environ. 277 (2020), 119136.
[17] S. Yang, X. Qiu, P. Jin, M. Dzakpasu, X.C. Wang, Q. Zhang, L.u. zhang, L. Yang, D. Ding, W. Wang, K. Wu, MOF-templated synthesis of $CoFe_2O_4$ nanocrystals and its coupling with peroxymonosulfate for degradation of bisphenol A, Chem. Eng. J. 353 (2018) 329–339.
[18] M. Abdul Nasir Khan, P. Kwame Klu, C. Wang, W. Zhang, R. Luo, M. Zhang, J. Qi, X. Sun, L. Wang, J. Li, Metal-organic framework-derived hollow $Co_3O_4$/carbon as efficient catalyst for peroxymonosulfate activation, Chem. Eng. J. 363 (2019) 234–246.
[19] C. Zhu, F. Liu, C. Ling, H. Jiang, H. Wu, A. Li, Growth of graphene-supported hollow cobalt sulfide nanocrystals via MOF-templated ligand exchange as surface-

bound radical sinks for highly efficient bisphenol A degradation, Appl. Catal. B Environ. 242 (2019) 238–248.
[20] D. Liu, M. Li, X. Li, F. Ren, P. Sun, L. Zhou, Core-shell Zn/Co MOFs derived $Co_3O_4$/CNTs as an efficient magnetic heterogeneous catalyst for persulfate activation and oxytetracycline degradation, Chem. Eng. J. 387 (2020), 124008.
[21] Y. Liu, W. Miao, Y. Feng, X. Fang, Q. Li, N. Du, D. Wang, S. Mao, Enhanced peroxydisulfate oxidation via Cu(III) species with a Cu-MOF-derived Cu nanoparticle and 3D graphene network, J. Hazard. Mater. 403 (2021), 123691.
[22] Y. Jing, M. Jia, Z. Xu, W. Xiong, Z. Yang, H. Peng, J. Cao, Y. Xiang, C. Zhang, Facile synthesis of recyclable 3D gelatin aerogel decorated with MIL-88B(Fe) for activation peroxydisulfate degradation of norfloxacin, J. Hazard. Mater. 424 (2022), 127503.
[23] Y. Bao, W. Oh, T. Lim, R. Wang, R.D. Webster, X. Hu, Surface-nucleated heterogeneous growth of zeolitic imidazolate framework – a unique precursor towards catalytic ceramic membranes: synthesis, characterization and organics degradation, Chem. Eng. J. 353 (2018) 69–79.
[24] Y. Li, X. Yan, X. Hu, R. Feng, M. Zhou, Trace pyrolyzed ZIF-67 loaded activated carbon pellets for enhanced adsorption and catalytic degradation of Rhodamine B in water, Chem. Eng. J. 375 (2019), 122003.
[25] L. Yang, M.A. Carreon, Deoxygenation of palmitic and lauric acids over Pt/ZIF-67 membrane/zeolite 5A bead catalysts, ACS Appl. Mater. Inter. 9 (37) (2017) 31993–32000.
[26] N. Li, G. Chen, J. Zhao, B. Yan, Z. Cheng, L. Meng, V. Chen, Self-cleaning PDA/ZIF-67@PP membrane for dye wastewater remediation with peroxymonosulfate and visible light activation, J. Membrane Sci. 591 (2019), 117341.
[27] M.-P. Zhu, J.-C. Yang, X. Duan, D.-D. Zhang, S. Wang, B. Yuan, M.-L. Fu, Interfacial $CoAl_2O_4$ from ZIF-67@γ-$Al_2O_3$ pellets toward catalytic activation of peroxymonosulfate for metronidazole removal, Chem. Eng. J. 397 (2020) 125339, https://doi.org/10.1016/j.cej.2020.125339.
[28] H. Chen, J. Wang, MOF-derived $Co_3O_4$-C@FeOOH as an efficient catalyst for catalytic ozonation of norfloxacin, J. Hazard. Mater. 403 (2021), 123697.
[29] M. Zhu, J.E. Yang, X. Duan, S. Wang, D.D. Sun, B. Yuan, M. Fu, Engineered $Co_2AlO_4$/$CoAl_2O_4$@$Al_2O_3$ monolithic catalysts for peroxymonosulfate activation: $Co^{3+}/Co^{2+}$ and $O_{Defect}/O_{Lattice}$ ratios dependence and mechanism, Chem. Eng. J. 409 (2021), 128162.
[30] X. Duan, C. Su, J. Miao, Y. Zhong, Z. Shao, S. Wang, H. Sun, Insights into perovskite-catalyzed peroxymonosulfate activation: maneuverable cobalt sites for promoted evolution of sulfate radicals, Appl. Catal. B Environ. 220 (2018) 626–634.
[31] J.E. Yang, M. Zhu, X. Duan, S. Wang, B. Yuan, M. Fu, The mechanistic difference of 1T–2H $MoS_2$ homojunctions in persulfates activation: structure-dependent oxidation pathways, Appl. Catal. B Environ. 297 (2021), 120460.
[32] L. Chen, H. Ji, J. Qi, T. Huang, C. Wang, W. Liu, Degradation of acetaminophen by activated peroxymonosulfate using $Co(OH)_2$ hollow microsphere supported titanate nanotubes: insights into sulfate radical production pathway through $CoOH^+$ activation, Chem. Eng. J. 406 (2021), 126877.
[33] O. Jones, N. Voulvoulis, J. Lester, Aquatic environmental assessment of the top 25 english prescription pharmaceuticals, Water Res. 36 (20) (2002) 5013–5022.
[34] R. Rosal, A. Rodríguez, J.A. Perdigón-Melón, A. Petre, E. García-Calvo, M. J. Gómez, A. Agüera, A.R. Fernández-Alba, Occurrence of emerging pollutants in urban wastewater and their removal through biological treatment followed by ozonation, Water Res. 44 (2) (2010) 578–588.
[35] J.E. Yang, B. Yuan, H. Cui, S. Wang, M. Fu, Modulating oxone-$MnO_x$/silica catalytic systems towards ibuprofen degradation: insights into system effects, reaction kinetics and mechanisms, Appl. Catal. B Environ. 205 (2017) 327–339.
[36] S. Giannakis, K.A. Lin, F. Ghanbari, A review of the recent advances on the treatment of industrial wastewaters by sulfate radical-based advanced oxidation processes (SR-AOPs), Chem. Eng. J. 406 (2021), 127083.
[37] L. Lian, B.o. Yao, S. Hou, J. Fang, S. Yan, W. Song, Kinetic study of hydroxyl and sulfate radical-mediated oxidation of pharmaceuticals in wastewater effluents, Environ. Sci. Technol. 51 (5) (2017) 2954–2962.
[38] T. Tandarić, V. Vrček, D. Šakić, A quantum chemical study of HOCl-induced transformations of carbamazepine, Org. Biomol. Chem. 14 (46) (2016) 10866–10874.
[39] S. Luo, Z. Wei, D.D. Dionysiou, R. Spinney, W.-P. Hu, L. Chai, Z. Yang, T. Ye, R. Xiao, Mechanistic insight into reactivity of sulfate radical with aromatic contaminants through single-electron transfer pathway, Chem. Eng. J. 327 (2017) 1056–1065.
[40] M.P. Rayaroth, K.P. Prasanthkumar, Y. Kang, C. Lee, Y. Chang, Degradation of carbamazepine by singlet oxygen from sulfidized nanoscale zero-valent iron – citric acid system, Chem. Eng. J. 382 (2020), 122828.
[41] G. Xiao, T. Xu, M. Faheem, Y. Xi, T. Zhou, H.T. Moryani, J. Bao, J. Du, Evolution of singlet oxygen by activating peroxydisulfate and peroxymonosulfate: a review, Int. J. Env. Res. Pub. He. 18 (2021) 3344.
[42] P. Duan, X. Liu, B. Liu, M. Akram, Y. Li, J. Pan, Q. Yue, B. Gao, X. Xu, Effect of phosphate on peroxymonosulfate activation: accelerating generation of sulfate radical and underlying mechanism, Appl. Catal. B Environ. 298 (2021), 120532.
[43] J.E. Yang, Y. Lin, H. Peng, B. Yuan, D.D. Dionysiou, X. Huang, D. Zhang, M. Fu, Novel magnetic rod-like Mn-Fe oxycarbide toward peroxymonosulfate activation for efficient oxidation of butyl paraben: Radical oxidation versus singlet oxygenation, Appl. Catal. B Environ. 268 (2020), 118549.
[44] F. Pan, H. Ji, P. Du, T. Huang, C. Wang, W. Liu, Insights into catalytic activation of peroxymonosulfate for carbamazepine degradation by $MnO_2$ nanoparticles in-situ anchored titanate nanotubes: mechanism, ecotoxicity and DFT study, J. Hazard. Mater. 402 (2021) 123779, https://doi.org/10.1016/j.jhazmat.2020.123779.
[45] L. Wang, X.u. Lan, W. Peng, Z. Wang, Uncertainty and misinterpretation over identification, quantification and transformation of reactive species generated in catalytic oxidation processes: a review, J. Hazard. Mater. 408 (2021) 124436, https://doi.org/10.1016/j.jhazmat.2020.124436.
[46] Y. Zhou, J. Jiang, Y. Gao, J. Ma, S. Pang, J. Li, X. Lu, L. Yuan, Activation of Peroxymonosulfate by benzoquinone: a novel nonradical oxidation process, Environ. Sci. Technol. 49 (2015) 12941–12950.
[47] E. Yun, J.H. Lee, J. Kim, H. Park, J. Lee, Identifying the nonradical mechanism in the peroxymonosulfate activation process: singlet oxygenation versus mediated electron transfer, Environ. Sci. Technol. 52 (2018) 7032–7042.
[48] S. Mo, Q.i. Zhang, Q. Ren, J. Xiong, M. Zhang, Z. Feng, D. Yan, M. Fu, J. Wu, L. Chen, D. Ye, Leaf-like Co-ZIF-L derivatives embedded on $Co_2AlO_4$/Ni foam from hydrotalcites as monolithic catalysts for toluene abatement, J. Hazard. Mater. 364 (2019) 571–580.
[49] R. Franco, F. Tielens, M. Calatayud, J.M. Recio, Cation distributions on $CoAl_2O_4$ and $Co_2AlO_4$ spinels: pressure and temperature effects, High Pressure Res. 28 (2008) 521–524.
[50] D.A. Pawlak, K. Woźniak, Z. Frukacz, T.L. Barr, D. Fiorentino, S. Seal, ESCA studies of yttrium aluminum garnets, J. Phys. Chem. B. 103 (9) (1999) 1454–1461.
[51] J. Bao, X. Zhang, B.o. Fan, J. Zhang, M. Zhou, W. Yang, X. Hu, H. Wang, B. Pan, Y. i. Xie, Ultrathin spinel-structured nanosheets rich in oxygen deficiencies for enhanced electrocatalytic water oxidation, Angew. Chem. Int. Edit. 54 (25) (2015) 7399–7404.
[52] J. Cao, S. Sun, X. Li, Z. Yang, W. Xiong, Y. Wu, M. Jia, Y. Zhou, C. Zhou, Y. Zhang, Efficient charge transfer in aluminum-cobalt layered double hydroxide derived from Co-ZIF for enhanced catalytic degradation of tetracycline through peroxymonosulfate activation, Chem. Eng. J. 382 (2020), 122802.
[53] Q. Qin, T. Liu, J. Zhang, R. Wei, S. You, Y. Xu, Facile synthesis of oxygen vacancies enriched α-$Fe_2O_3$ for peroxymonosulfate activation: a non-radical process for sulfamethoxazole degradation, J. Hazard. Mater. 419 (2021), 126447.
[54] Y. Wang, M. Liu, C. Hu, Y. Xin, D. Ma, M. Gao, H. Xie, Enhanced $MnO_2$/peroxymonosulfate activation for phthalic acid esters degradation: Regulation of oxygen vacancy, Chem. Eng. J. 433 (2022) 134048, https://doi.org/10.1016/j.cej.2021.134048.
[55] X. Long, C. Feng, D. Ding, N. Chen, S. Yang, H. Chen, X. Wang, R. Chen, Oxygen vacancies-enriched $CoFe_2O_4$ for peroxymonosulfate activation: the reactivity between radical-nonradical coupling way and bisphenol A, J. Hazard. Mater. 418 (2021), 126357.
[56] R. Xiao, J. Ma, Z. Luo, W. Zeng, Z. Wei, R. Spinney, W.P. Hu, D.D. Dionysiou, Experimental and theoretical insight into hydroxyl and sulfate radicals-mediated degradation of carbamazepine, Environ. Pollut. 257 (2020), 113498.
[57] L. Lai, H. Ji, H. Zhang, R. Liu, C. Zhou, W. Liu, Z. Ao, N. Li, C. Liu, G. Yao, B. Lai, Activation of peroxydisulfate by V-Fe concentrate ore for enhanced degradation of carbamazepine: surface ≡V(III) and ≡V(IV) as electron donors promoted the regeneration of ≡Fe(II), Appl. Catal. B Environ. 282 (2021), 119559.
[58] G.P. Anipsitakis, D.D. Dionysiou, M.A. Gonzalez, Cobalt-mediated activation of peroxymonosulfate and sulfate radical attack on phenolic compounds. implications of chloride ions, Environ. Sci. Technol. 40 (3) (2006) 1000–1007.
[59] J. Costanza, D.G. Lynch, R.S. Boethling, J.A. Arnot, Use of the bioaccumulation factor to screen chemicals for bioaccumulation potential, Environ. Toxicol. Chem. 31 (10) (2012) 2261–2268.
[60] M. Xu, J. Deng, A. Cai, C. Ye, X. Ma, Q. Li, S. Zhou, X. Li, Synergistic effects of UVC and oxidants (PS vs. chlorine) on carbamazepine attenuation: mechanism, pathways, DBPs yield and toxicity assessment, Chem. Eng. J. 413 (2021), 127533.